GATING AND PERMEATION IN ION CHANNELS

by

Joe Warren Dukes, Jr

B.S. in Chemistry, Winthrop University, 2001

Submitted to the Graduate Faculty of

College of Arts and Sciences in partial fulfillment

of the requirements for the degree of

M.S. in Chemistry

University of Pittsburgh

2004

UNIVERSITY OF PITTSBURGH

FACULTY OF ARTS AND SCIENCES

This dissertation was presented

by

Joe Warren Dukes, Jr

It was defended on

November 18, 2004

and approved by

Kenneth Jordan, PhD, Professor

Gilbert Walker, PhD, Associate Professor

Thesis Advisor: Rob Coalson, PhD, Professor

GATING AND PERMEATION IN ION CHANNELS

Joe Warren Dukes, Jr

University of Pittsburgh, 2004

Recent crystal structures of ClC chloride channels have led to a proposed fast-gating mechanism that couples ion permeation to ion channel gating. This proposed mechanism is studied by pushing the amino acid E148 of StClC out of the path of the proposed permeation path. The resulting structure produces an open state that is similar to the mutant EcClC E148Q structure, a proposed open structure of ClC-type channels. Due to the interaction of the fast-gate with permeating ions, a hybrid methodology is proposed for explicitly simulating the interaction of protein fluctuations with permeating ions. This methodology is used for two model systems and compared to single-ion Potential of Mean Force permeation models methodologies.

TABLE OF CONTENTS

LIST OF FIGURES

1. Opening ClC and Fast Gating

1.1. Introduction to ClC

There is a great deal of interest in studying the function of ClC channels, especially since high resolution crystal structures has been determined (Dutzler et al., 2002). ClC is a family of ion channels that typically regulate the flow of chloride ions; they were first discovered in 1980 (Miller et al., 1980). Chloride channels play critical roles in regulating the resting potential of muscles, electrical excitability, regulating cell size, and renal and intravascular ion transport. Chloride channels are found in all forms of life.

The structure of ClC channels is significantly different than that of any other known ion channel. A single ClC channel is a dimer composed of two ion conducting pores (Miller et al., 1984), which was confirmed by the crystal structures (Figure 1; Dutzler et al., 2002). In Figure 1, a chloride ion (colored green) is bound in the crystal structure in each pore, near the center of the pore. Each monomer contains a chloride conducting pore, which is roughly denoted in Figure 2 (Dutzler et al., 2002).

As seen in Figure 1b, there are many alpha helices that only partially cross the membrane, in contrast to the common view of transmembrane proteins being composed of helices that completely traverse the width of the membrane. Also, unlike gramicidin A, KscA, and alpha-Hemolysin, there is no easily identified pore that lies along an axis of symmetry (Doyle et al., 1998; Arseniev et al., 1992; Song et al., 1998). Note that each monomer of the chloride channel is roughly anti-parallel and dimeric, as seen in Figure 3. This is in stark contrast to the KscA potassium channel, which is parallel and contains a large aqueous cavity (Doyle et al., 1998).

ClC channels commonly are gated via two different mechanisms. One mechanism is termed the "slow-gate" and involves cooperative gating between both pores (i.e. when the slow-gate is closed, neither pore can conduct chloride ions) (Miller et al., 1984). Typical slow gating times are on the order of seconds, for example ClC-0 slow-gate open times are typically 10-100 seconds (Miller et al., 1982, Pusch et al., 1997). Figure 4 is a cartoon sketch (Miller et al., 1984) of the slow-gating mechanism.

The second gating mechanism in ClC is the "fast gate." Miller et al. (1984) deduced from current measurements of ClC-0 that there exists a fast-gate for each pore, and each fast gate acts independently. The typical mean dwell time for the fast gate of ClC-0 is 0.3 ms (Miller et al., 1984). A well conserved glutamate residue in the pore of the channel plays a pivotal role in fast-gating behavior (Dutzler et al., 2003). This residue shows up in a critical location in the crystal structure (Figure 5): it is obstructing the chloride permeation path (Dutzler et al., 2002). Thus, it appears that for ion conduction to occur, this glutamate "gate" must swing out of the ion conduction pathway. Pusch et al. (1995) discovered that the extracellular concentration of chloride ions strongly affects the open probability of the channel. Pusch et al. concluded that the permeating chloride ions control the fast gating of a particular pore.

The focus of our research is studying ion permeation in ClC. However, the two crystal structures of ClC (StClC and EcClC) published in 2002 both have the glutamate gate positioned in the closed state. Also, because the fast-gate is so strongly coupled to ion permeation, any insight into the function of the fast gate will be valuable in studying permeation. Thus, our first task in studying ClC was to obtain an open structure for ClC, which involves moving (and to some extent, modeling) the fast gate. In section 1.2, a simple approach for opening the gate is presented, where a chloride ion is moved from the intracellular side of the channel to the

extracellular side of the channel. The opened structure for the ClC channel and the two states (opened and closed) of the glutamate gate are discussed in sections 1.3 and 1.4. In section 2, a model for coupling the gating motion with ion permeation is presented (a hybrid Monte-Carlo, Brownian Dynamics scheme abbreviated as MC/BD). This model is developed in section 2.2, and, in section 2.3 it is compared to /Poisson-Nernst-Planck (PMF/PNP) calculations and PMF/Brownian dynamics (PMF/BD) simulations for two simple systems (PMF/PNP and PMF/BD theory and methods are discussed in section 2.2). Future work on fast gating energetics and extension of the MC/BD model is discussed in section 3.

1.2. Method for Opening the Channel

1.2.1. Overview of Channel Opening Method

Because the glutamate gate in both crystal structures (Dutzler et al., 2002) is blocking the pore, it is necessary to "move" it out of the permeation path. Because channel opening is strongly correlated to extracellular concentration and the glutamate gate (Pusch et al., 1995; Chen et al., 2001), an initial hypothesis for the opening mechanism (Jentsch, 2002) was that electrostatic repulsion between the glutamate gate and a chloride ion would force the gate out of the permeation path (possibly with the assistance of an externally applied electric field and by multiple chloride ions). To achieve this gating motion, we placed the chloride ion on one side of the pore and brought the simulation system to thermodynamic equilibrium via molecular dynamics (MD). Then the chloride ion was moved by a small increment, closer to the glutamate gate, and the system was re-equilbrated. This process of moving the ion in small increments and

re-equilibrating the system with the chloride ion position fixed was repeated, eventually forcing the glutamate residue out of the path of the permeation path.

1.2.2. Details of Opening the Channel

For these calculations, the StClC (pdb code 1KPL) crystal structure found by Dutzler et al. (2002) was used. Sulfate ions, octane molecules, and pentadecane molecules were removed from the crystal structure (sulfate, octane, and pentadecane are present to assist in crystallizing StClC; Dutzler et al., 2002). Also, in the StClC structure, residues 1-30 and 461-473 of one monomer (chain A) and 1-11 and 463-473 of the other monomer (chain B) are missing. Thus, residues 12-30 and 461-462 from the structure of chain B were removed. These residues were removed from the structure for the following reasons: 1) so that chains A and B are structurally symmetric, 2) the StClC has an overall positive charge, and the residues 12-30 are composed of net positive charge (for MD simulations, a system net charge of zero is desired, especially for periodic boundary conditions), and 3) the residues removed from chain B are sufficiently far away from the selectivity filter and the glutamate gate; that it is unlikely they play a significant role in fast gating. Also, 6 additional chloride ions were added to the water reservoir of the system to neutralize the charge of the system. As seen in Figure 1, ClC has a rhombic shape when looking down on the membrane. A periodic system whose unit cell is a rhomboidal prism, producing an infinite layer of ClC channels packed together, was constructed. The rationale for this setup is that we are primarily interested in the pore region of the channel, and this pore region is far enough away from the membrane that the membrane does not significantly affect the structure or function of the pore region. The system was solvated with water molecules

(using the TIP3P model). The time-step for the simulations was 2 fs, with all covalent hydrogen bonds fixed, and using a non-bonded cutoff radius of 10 Angstroms for non-bonded interactions. NAMD2 (Kalé et al., 1999) was used to perform the molecular mechanics energy minimizations and molecular dynamics. The CHARMM 22 force field (MacKerell et al., 1998; Schlenkrich et al., 1996) was employed. Initially, the 27,751 atom solvated system with chloride ions at the original crystal structure position was brought to equilibrium at constant temperature and pressure for 1 ns using particle mesh Ewald (PME) sums for long range electrostatic interactions. After initial equilibration, the ion was placed in the intracellular reservoir, approximately 13 Å away from its original position and its z coordinate was fixed (the z axis is roughly normal to the plane of periodic ClC channels). The remaining simulations were performed with chain B of the ClC channel fixed and with the volume held constant. The system was then brought to equilibrium with 260 ps of MD simulation (the last 200 ps of simulation was used for gathering statistics). Then, the z coordinate of the chloride ion was changed by 1 Å to move the chloride ion closer to the extracellular side of the channel, and the equilibrium process was repeated. Also, analogous calculations were carried out for opening the channel by moving the chloride ion from the extracellular to the intracellular side of the channel.

1.3. Results of the Channel Opening

In 2003, Dutzler et al. published more detailed crystal structures of the gating regions of EcClC, where the wild-type EcClC was, once again, crystallized in the closed state. However, two mutant proteins (one where the glutamate is mutated to an alanine and in the other the glutamate was mutated to glutamine, E148Q) were crystallized with the gating side chain no

longer protruding into the pore (Figure 7). The E148Q structure is of particular interest because glutamate and glutamine have essentially the same geometry; however, at neutral pH, glutamate has a negative charge and glutamine is neutral. In our calculations, there exist two distinct states of the glutamate side chain for the intracellular to extracellular opening trajectory (Figure 8). The glutamate side chain's initial state in our calculations correlates well to the closed crystal structure (StClC), while the final state identified by our calculations correlates well to the open state (E148Q) found by Dutlzer et al. (2003). Thus, the intracellular to extracellular trajectory is consistent with a two-state process whose reaction coordinate is characterized well by the side chain dihedral angles. When we examined the glutamate gate's backbone (the backabone alpha-carbon root mean square displacements [RMSD]; Figure 6), the intracellular to extracellular opening trajectory produced minimal deviations in the glutamate backbone position, suggesting that the intracellular to extracellular trajectory does not produce any long range conformational changes.

In contrast, when we examined the side chain dihedrals of the glutamate gate, the trajectory produced by moving the chloride ion from extracellular side to the intracellular side of the channel did not produce two distinct states (as one might expect two distinct states corresponding to the open state and the closed state). Furthermore, the final state does not correlate well with the open state proposed by Dutzler et al. (2003). Also, when examining the RSMD of the glutamate backbone (Figure 6) along the extracellular to intracellular trajectory (Figure 6), it appears that the glutamate residue moves a significant distance, causing the backbone to be distorted and causing more significant conformational changes than simple glutamate side chain motions. The odd side chain configurations of the extracellular to intracellular trajectory coupled with the large deviations of the backbone drastically diminish the

likelihood that an extracellular to intracellular chloride trajectory produces the open structure. The comparison of the two opening trajectories presented here is consistent with Dutlzer et al.'s (2003) proposed open structure (Figures 7 and 9).

The open structure we generated from the intracellular to extracellular opening trajectory did not result in a fully solvated pore, with a line or "string" of connected water molecules. Thus, to identify the pore, an MD snapshot with a chloride ion in the middle of the pore was chosen, and water molecules were added around it, to solvate the pore. Then the system was equilibrated for 500 ps at constant volume and temperature. This yielded a solvated pore with a string of water molecules; however, there is a branch in the solvation pore on the intracellular side (Figures 10 and 11). The branching point at residue Y445 (shown in Figures 10 and 11) emphasizes the importance of this highly conserved residue in the ClC family (Dutzler et al., 2003). The importance of Y445 (in conjunction with S107, not shown here) has been noted in recent MD simulations by Cohen et al. (2004) and in experiments on ClC-0 by Accardi et al. (2003). However, the role of Y445 and S107 in selectivity and/or gating is not yet clear.

Poisson-Nernst-Planck (PNP; see section 2.2.2 for more details of PNP theory) calculations (not shown here) on several snapshots of the open structure confirm that the channel is anion selective; but, the rectification and currents produced by PNP are very sensitive to the pore structure. Thus, PNP calculations using MD trajectory snapshots separated by small time increments produce a wide range of rectifications of anionic currents.

1.4. Discussion of Opening the Channel

Pusch et al. (1995) demonstrated that increasing the extracellular chloride concentration increases the open probability. However, it was not until 2003 that Chen et al. demonstrated the relationship of intracellular and extracellular chloride concentrations to fast gating. Chen et al. found that increased extracellular chloride concentration increases the opening rate, while increased intracellular chloride concentration has no effect on the opening rate. The opposite is true for the closing rate: increasing the intracellular concentration decreases the closing rate while the extraceullular concentration has little effect. Thus, it is unlikely that the procedure for opening the gate by moving a chloride ion from the intracellular to extracellular side of the channel is indicative of the actual mechanism for opening the gate; in fact, it isn't clear at all how the gate is opened (Chen et al., 2003).

To shed light on this gating mechanism, we will compute the potential of mean force (PMF) for the for the negatively charged glutamate gate as a function of the two dihedral angles of the side chain. By computing this PMF with the chloride ions in several different positions (extracellular and intracellular), it may be possible to elucidate the specific mechanism by which the gate opens, and provide more insight into the closing mechanism (Chen et al., [2003] proposed a foot in the door mechanism for closing). Also, there is relationship between the pH, charge of the gating residue, and gating motions (Chen et al., 2001, Dutzler et al., 2003). It has been proposed that a fast gating mechanism involves protonating the glutamate residue, thus decreasing the binding affinity of the glutamate gate in the closed position (where a large positive electrostatic potential is located between two alpha-helix dipoles) (Miloshevsky et al.,

2004; Yin et al.; Dutzler et al., 2003). We can also perform PMF calculations of the glutamate gate with no net charge (in addition to the negatively charged glutamate) in order to determine the role of the protonation state of glutamate in the gating mechanism.

Because the fast-gating of the channel is closely coupled to ion permeation, the fast gate should be considered when studying permeation. Typically ion permeation is studied using a "static" structure for the protein, for example in PNP calculations and BD simulations. The difficulty in obtaining reliable results for PNP calculations on the opened structure of StClC emphasizes the underlying problem of using a static structure for studying this channel family and the degree to which currents predicted depend on the structure of the channel. In order to study ion-permeation coupled with gating, a new model for studying ion permeation is proposed: Brownian dynamics with a dynamical gate. This methodology will be explored in depth in the remainder of this document. Using this methodology coupled with the preliminary work on the permeation pathway of ClC outlined above, it will be possible to create an atomically detailed model of ion-permeation that explicitly considers the fast-gating motion.

2. MC/BD: Coupling Permeation to Fast Gating

2.1. Introduction to MC/BD

When studying ion-permeation through ion channels, the flow of ions usually is assumed not to be coupled to gating motions of the channel (which are typically on a longer time scale than permeation events). Thus, it is common to study ion permeation using static structures for the ion channel. However, protein fluctuations often play a crucial role in stabilizing the ion in

the pore (Mamonov et al., 2003; Roux et al., 2002). Brute force molecular dynamics (MD) simulation is one method used to determine protein fluctuations. However, both the time scale needed to collect accurate statistics and the size of the systems makes using MD to study ion permeation impractical for all but the simplest systems (although some attempts have been made: Crozier et al., 2001). Consequently, the potential of mean force (PMF) for ions permeating through ion channels were calculated and used in BD simulations (Im et al., 2000) and later PNP calculations (Mamonov et al., 2003).

However, calculating single-ion PMF's (PMF's that are a function of a single ion coordinate) is a difficult task. It can be hard to obtain good convergence, even when using methods like umbrella sampling (Valleau et al., 1972; Roux, 1995) and the weighted histogram analysis method (WHAM: Kumar et al., 1992). Thus, calculating accurate PMF's requires a large amount of CPU time, and if ion permeation involves multiple-ions interacting in the pore, a multi-ion PMF must be calculated (requiring even more CPU time to explore the additional degrees of freedom). Also, a PMF is typically calculated at equilibrium, where ion-permeation is typically a non-equilbrium event (for example, PMF's calculated at equilibrium do not take into account the ion-channel interacting with the externally applied field which typically drives ion conduction; typically, however, this perturbation is small). Another issue is that a single-ion PMF may be inadequate for describing the interaction of a single, permeating ion interaction with the gate of ClC (discussed later in section 2.2.9).

Hence, a hybrid Monte-Carlo/Brownian Dyanmics approach to modeling ClC is proposed. In this approach, the key protein fluctuation/gating motion is modeled with the Metropolis Monte-Carlo algorithm while Brownian dynamics is used for simulating ion trajectories. Using Metropolis Monte-Carlo for the gate assumes that the gate is always in local

equilibrium with its surroundings, which is the same assumption made to justify using single-ion or multi-ion in dynamical simulations (such as BD).

However, before performing MC/BD simulations of ClC, it is necessary to test the MC/BD methodology. Thus, for two simple model systems, the explicit MC/BD model is compared to PNP calculations and BD simulations that utilized single-ion PMF's (PMF/PNP and PMF/BD).

2.2. Theory and Methods

2.2.1. Theory: PMF

First the mean force (MF) is defined as:

$$< \vec{F}_i >= \frac{\int (-\vec{\nabla}_i U(\vec{r}_i, c^N)) e^{-\frac{U(\vec{r}_i, c^N)}{kT}} dc^N}{\int e^{-\frac{U(\vec{r}_i, c^N)}{kT}} dc^N}$$

where $\vec{F}_i$ is the force acting on particle i, $\vec{r}_i$ is the position of particle i, c^N is all the remaining coordinates of the system, U is the interaction potential of the system, k is Boltzmann's constant, and T is the absolute temperature (McQuarrie 1976). The difference in PMF of particle i at positions $\vec{r}_{i1}$ and $\vec{r}_{i2}$ is defined as:

$$PMF_i(\vec{r}_{i2}) - PMF_i(\vec{r}_{i1}) = -\int_{\vec{r}_{i1}}^{\vec{r}_{i2}} < \vec{F}_i > \cdot d\vec{r}_i$$

where the MF is integrated along a path connecting positions $\vec{r}_{i1}$ and $\vec{r}_{i2}$ (Chandler 1987, Kirkwood, 1935). This difference in PMF at two positions is also equal to the reversible work for moving particle i from position $\vec{r}_{i1}$ to position $\vec{r}_{i2}$. The reversible work theorem relates the PMF at a position to the probability of the particle existing at that position (Chandler 1987):

$$p(\vec{r}) \propto e^{-\frac{PMF(\vec{r})}{kT}}$$

The most common method of calculating PMF from molecular dynamic trajectories is to use the reversible work theorem.

2.2.2. Theory: PNP

PNP involves coupling the Poisson Equation to the Nernst-Planck Equation. A set of N Nernst-Planck equations for species i=1,2,…,N

$$\vec{j}_i(\vec{r},t) = -D_i(r)[\vec{\nabla}c_i(\vec{r},t) + \beta c_i(\vec{r},t) z_i e \vec{\nabla}\phi(\vec{r},t)]$$

is solved at steady state

$$div(\vec{j}_i) = 0$$

for the ionic concentrations, c_i (i is the ionic species, D_i is the diffusion constant, $\beta = 1/k_bT$, k_b is the Boltzmann constant, T is the temperature in Kelvin, e is the charge of proton, z_i is the valence of the ionic species i, and $\vec{j}_i$ is the flux of this species) (Kurnikova et al., 1999; Cardenas et al., 2000). The electrostatic potential, ϕ is determined by solving the Poisson equation

$$\vec{\nabla} \cdot [\varepsilon(\vec{r})\nabla\phi(\vec{r})] = -4\pi \sum_i z_i c_i(\vec{r})$$

where ε is the dielectric constant. The Poisson and Nernst-Planck equations are solved self-consistently.

2.2.3. Theory: MC/BD

Brownian dynamics is the description of seemingly random motions of solute particles in solvent. This stochastic process is described by the Langevin Equation:

$$m\frac{d^2\vec{r}(t)}{dt^2} = \vec{F} - \gamma\frac{d\vec{r}(t)}{dt} + \vec{f}(t)$$

where m is the mass of the solute particle of interest, $\vec{r}$ is its position, $\vec{F}$ is the systematic force acting on the particle, γ is the friction constant of the particle in the solvent, and $\vec{f}$ is the random force due to collisions with the implicitly represented solvent (McQuarrie 1976, Chandrasekar 1943). Assuming a large friction constant (overdamped regime), the left hand side of the Langevin Equation becomes 0, and the velocity of the particle is then:

$$\frac{d\vec{r}(t)}{dt} = \frac{1}{\gamma}(\vec{F} + \vec{f}(t))$$

where the friction constant is related to the diffusion constant by the Stokes-Einstein relation, D = kT/ γ. For hybrid PMF/BD calculations, the force $\vec{F}$ is the mean force ($<\vec{F}>$) on the solute particle computed from the gradient of the PMF. For MC/BD calculations, the force $\vec{F}$ is computed from the bare intermolecular potential for the system.

For modeling protein/gate fluctuations, the Metropolis Algorithm acceptance criteria is used for accepting random moves of the gate. That is, a trial move is accepted if:

$$R \leq \exp(-\frac{\Delta U}{kT})$$

where R is a uniformly distributed random number between 0 and 1, and ΔU is the change in the energy of the system due to the trial move (the energy of the trial configuration minus the energy of the previously accepted configuration) (Leach 2001).

2.2.4. Methods: Maintaining Constant Concentration and BD Details

In order to maintain constant concentration "far away" from the membrane, each reservoir was separated into two sections (Figure 12). The gray shaded regions are the "buffer" regions, where a constant number of particles are maintained by counting the number of particles in the buffer every 10^5 simulation steps, and destroying or creating particles in order to obtain the desired concentration. When creating particles, all particle creation events that add more than 3kT of energy to the system are rejected.

Also, we employ a dual time-step scheme was used, with a 100 fs time-step for the reservoir region and a 10 fs time-step for the pore region (Chung et al., 2001). Periodic boundary conditions are used for a system measuring 100x40x40 Å (the longest dimension corresponding to the channel axis). To model volume exclusion (and hard sphere potential), if, during a BD move, a particle collides with another particle, membrane wall, or pore wall, the move is rejected and the particle is moved back to its location prior to the attempted BD move, completing its move for the designated time-step. A 15 Å cutoff is used when calculating pair-wise interactions, based on a neighbor interaction list that is updated when any particle in the system moved 2.5 Å from its position at the time of the last neighbor list update.

2.2.5. Methods: Common System Parameters

The system consists of a uniform dielectric constant, a membrane modeled by a rectangular slab from which ions are excluded, and an ion permeable pore through the membrane. The calculation parameters used are: membrane thickness 33 Å, dielectric constant 80 (assuming a homogenous dielectric environment constitutes a severe over- simplification of the real, biological system; however, this approximation is taken to simplify the calculations and for making comparisons between the different levels of theory as direct as possible), diffusion constant for cations and anions of $2x10^{-5}$ cm^2/s, pore radius of 2 Angstroms, and ionic concentrations of 0.14 M. Applied potentials used in the BD and PNP calculations were obtained by performing a Poisson calculation of an identical system (without ions) except that a membrane dielectric constant of 2 was used. The applied potential is then added to the PMF potential in the Nernst-Planck equation for PNP calculations, and the force generated by the applied potential was added to the force term of the Langevin equation for BD simulations. This procedure for calculating the applied potential is necessary for restricting the applied potential drop across the membrane region (in a homogenous dielectric environment, the potential drop would be linear across the entire system). PNP (and Poisson) calculations were performed on a 169x169x169, 3.0 grids/Å lattice.

2.2.6. Methods: Calculating PMF for Model Systems

The reversible work theorem was leveraged for computing the PMF of the model systems. Note that the mean force can be computed from the configuration integral:

$$\frac{d\left\{\ln\left(\int e^{-U(\vec{r}_1,\vec{r}_2)}d\vec{r}_2\right)\right\}}{d\vec{r}_1} = < \vec{F}_1 >$$

where $\vec{r}_1$ is the position of the permeating ion and $\vec{r}_2$ is the position of the model gate.

Thus, the difference in PMF at two permeating ion positions, $\vec{r}_1'$ and $\vec{r}_1''$, can be computed by computing the configuration integrals at the two permeating ion positions (where the position of the permeating ion is constrained):

$$PMF(\vec{r}_1'') - PMF(\vec{r}_1') = -\ln\left(\frac{\int e^{-U(\vec{r}_1'',\vec{r}_2)}d\vec{r}_2}{\int e^{-U(\vec{r}_1',\vec{r}_2)}d\vec{r}_2}\right)$$

The PMF was calculated on a three-dimensional grid with a scale of 3.0 grids/Å. The configuration integral an ion at a particular position was calculated by performing Monte-Carlo integration (randomly selecting 40 million points from the configurational space of the gate). The PMF was calculated at every lattice point in the pore.

2.2.7. Model System 1

The first model system considered is a charged particle attached to the wall of the pore by a spring (shown in Figure 13). The point where the spring is attached to the pore wall is the origin of the coordinate system. Particles 1 and 2 have a hard sphere potential, and thus the distance between particles 1 and 2 is greater than or equal to d_{vdw}. Thus, the potential for the system is:

$$U(\vec{r}_1,\vec{r}_2)=\begin{cases}\infty, \left|\vec{r}_2-\vec{r}_1\right| < d_{vdw} \\ \dfrac{1}{2}k_s {r_2}^2 + \dfrac{q_1 q_2}{\varepsilon\left|\vec{r}_2-\vec{r}_1\right|}, \left|\vec{r}_2-\vec{r}_1\right| \geq d_{vdw}\end{cases}$$

where k_s is the spring constant and q_1 and q_2 are the charges of particles 1 and 2, respectively. For the calculations of PMF and simulations, the spring constant k_s is 1 kT/Å^2, monovalent permeating ions with 1.5 Å radius were used, and the gate particle is a divalent anion with a 0.5 Å radius. A divalent anion was used for these simulations in order to produce a significant energy well in the channel for cations and significant energy barrier for anions; thus, emphasizing any differences in the treatment of interactions between mobile ions and the gate particle between PMF/PNP, PMF/BD, and MC/BD.

2.2.8. Model System 2

The second model system studied was a "swinging arm" model for the gate (as shown in Figure 14). Particle 2 is attached to a "swinging" bar. The swing bar is attached to the wall of the channel at the origin of the coordinate system. The bar is held perpendicular to the wall of the channel by a spring. The positions of particles 1 and 2 are $\vec{r}_1$ and $\vec{r}_2$, respectively. The angle between the swinging bar and the perpendicular, equilibrium position of the bar is θ. The bar is only allowed to swing in the plane of the diagram:

$$r_{2x} = d\sin(\theta)$$
$$r_{2y} = 0$$
$$r_{2z} = d\cos(\theta)$$

where d is the length of the bar (the distance between the origin of the system and the position of particle 2), which is a constant. Particles 1 and 2 are treated as hard spheres so that the distance between the particles, r_{12}, is never less than d_{vdw}. The potential of the system is:

$$U(\theta,\vec{r}_1)=\begin{cases}\infty, r_{12} < d_{vdw} \\ \frac{1}{2}k_s\theta^2 + \frac{q_1 q_2}{\varepsilon r_{12}}, r_{12} \geq d_{vdw}\end{cases}$$

where the spring constant k_s is 1 kT/radian^2, the length of the bar is 2 Å, and all other system parameters are the same as the first model system.

2.2.9. Methods: Why Study Model Systems 1 and 2?

In model system 1, the gate can move in 3 dimensions, allowing it to move around a permeating ion for any location of the permeating ion. Thus, performing MC moves on the gate should produce the same set of ensemble configurations as those randomly generated for computing the PMF of a permeating ion. However, in model system 2, the gate only has one degree of freedom, and if a permeating ion is blocking its path, the gate cannot physically jump over (or leap over) the permeating ion. Thus, the set of random configurations sampled by performing MC on the gate during a BD simulation is not necessarily the same set of configurations generated by the calculation of the PMF. As can be seen from Figure 15, the physically allowable set of configurations of the gate depends not only on the position of the permeating ion but also on the position of the gate; thus, invalidating the single-ion PMF because it does not explicitly account for the position of the gate. To test this hypothesis, we performed MC/BD calculations for model system 2 using small MC steps for modeling the gate (so that the gate is not allowed to leap over the permeating ion) and another set of MC/BD calculations using

large MC steps for the modeling the gate (so that the gate is allowed to leap over the permeating ion). For small moves the maximum distance the gate is allowed to move in a single step is 0.1 Å, and the maximum allowed for large MC steps is 4 Å. The hypothesis is that MC/BD calculations using large MC gate steps should produce similar results to PMF/BD and PMF/PNP calculations, while using small MC gate steps will produce results that diverge from the PMF/BD and PMF/PNP calculations.

Another motiviation for studying model system 2 is its relationship to the ClC channel. Model system 2's gating particle is analogous to the glutamate gate of the ClC channel. Both systems have a closed configuration where the gate blocks the passage of ions, and its open structure is obtained by swinging the gate out of the permeation path to location barried in the wall of the pore. Thus, it is likely that insight into the dynamics of the ClC fast gate can be obtained from studying model system 2.

2.3. Results

2.3.1. Results: Comparing Bare PNP and BD

As a starting point, it is useful to compare PNP and BD on a simple system composed of a membrane, a pore, and diffusing ions (but no gate). This system produces a good basis for comparing the results for model system 1 and model system 2 (where the effects of gate fluctuations are considered). Some BD simulations where performed without ion-ion interactions (coulomb and hard sphere); this is useful for determining the role ion-ion interactions play in calculating currents and concentration profiles.

As can be seen in Figure 16, PNP, BD with ion-ion interactions, and BD without ion-ion interactions produce very similar results. PNP produces a linear I-V curve, while BD with ion-ion interactions has a very slightly non-linear I-V curve. This non-linearity in the BD I-V curve disappears when ion-ion interactions are removed, thus highlighting a key difference in BD and PNP in that BD explicitly takes into account ion-ion interactions while PNP only accounts for them in a mean-field manner (this missing effect in PNP will be called "ion-ion correlation" for the remainder of this report). As can be seen from Figure 17, the concentration profiles for PNP and BD both show a relatively constant concentration through the pore and reservoirs. PNP and BD agree reasonably well.

2.3.2. Results: Model System 1

Using the PMF computed for model system 1 (Figure 18), it can be seen that PMF/BD produce similar I-V curves for both anions and cations in comparison to MC/BD (figure 19). Thus, MC samples the same equilibrium configurations that are used to compute the PMF. These results confirm that performing MC simulation on the gate between BD simulation steps is analogous to the approximation of fast protein relaxation used to justify the use of a single-ion PMF for BD calculations. When examining the PMF/PNP I-V curves, one sees that PMF/PNP overestimates the currents, especially in the case of the anionic currents. This scenario is similar, but exaggerated compared to what is seen in bare PMF and BD, where the ion-ion correlations of BD dampen the ionic currents. We suspect that this dampening of the currents is produced by the attractive interaction between positive and negative ions (if the hard sphere radius of the permeating ions is reduced to 1.0 Å, the dampening of currents due to ion-ion correlations effects is increased). It is noteworthy that all levels of theory produce the same relative trends. When

examining the concentration profiles (Figure 20), all the levels of theory produce the same concentration profiles.

2.3.3. Results: Model System 2

Using the PMF computed for model system 2 (Figure 21), the cation currents calculated by PMF/BD compare reasonably well to those computed by MC/BD. However, the anion currents produced by PMF/PNP diverge significantly from all the BD calculations. The effect of ion-ion correlations in the BD calculations has been further emphasized in model system 2, even more so than in model system 1. This increase of the ion-ion correlation effect is due to the deeper energy well for cations in model system 2 (the energy well is deeper because the equilibrium position of the gate for model system 2 is in the center of the channel as opposed to being on the wall of the pore, as is the case for model system 1). Therefore, in the PMF/PNP calculations, the large binding energy and concentration of ions causes a larger number of anions (Figure 23) to cross the pore due to the lower energy barrier for anions (caused by the large concentration of cations). However, this effect of lowering of the effective energy barrier for anions is not significant in the BD calculations due to the hard sphere potential between mobile-ions that is present in BD calculations.

Also, upon closer examination, MC/BD with big moves and PMF/BD agree rather well, while MC/BD with small moves produces significantly smaller anion currents. This confirms our hypothesis of a "leap frog" effect produced by PMF or MC with big moves that should be absent in MC/BD simulations with small moves.

When examining the concentration profiles (Figure 23), all the levels of theory produce the same concentration profiles.

2.4. Discussion of MC/BD

Both in the test case and in the model systems, one can see the failure of PNP and PMF/PNP to take into account ion-ion correlations. This failure is highlighted in the drastic divergence of the PMF/PNP results for anion currents in model system 2. Here one would predict (and the concentration profiles confirm) that the largest cation concentrations occur at the center of the channel, where the minimum of the cation PMF is located. This large cation concentration at the center of pore would cause a decrease in the effective free energy barrier for anions to cross the pore in PMF/PNP calculations (where ion-ion correlations are neglected). Consequently, the anion currents predicted for Model System 2 are significantly higher than currents predicted by PMF/BD and MC/BD calculations (which do take into account ion-ion correlations).

Clearly, if it is critical to account for ion-ion correlation effects, then taking into account ion-protein interactions explicitly is important as well when protein fluctuations are coupled and strongly interact with permeating ions. Note the weakness of PMF calculations to properly take into account the "accessible" equilibrium configurations for model system 2, where the single ion PMF cannot properly describe the interaction of the ions with the fluctuating gate particle. In model system 2, it is insufficient to describe the interaction between the ion and the gate by naively integrating over all conceivable configurations of the gate for a given ion position; the dynamics of this system must be taken into account. In particular, to accurately describe this system, the explicit position of the gate must be considered.

3. Future Work

We are currently computing the PMF of the glutamate gate as a function of the two side chain dihedral angles for the ClC channel. These PMF calculations can be performed also in the presence of ions at different locations. Thus, the explicit role of permeating ions in opening and closing the gate may be determined since it is known that chloride ions on the intracellular and the extracellular side of the pore function differently in this regard (see section 1.4 for further details). Also, the charge state can be changed on the glutamate gate to determine the role of pH on gating (Chen et al., 2003; Dutzler et al., 2003).

Armed with a more detailed picture of the glutamate gate dynamics and energetics, a more detailed model of the gating in ClC can be developed (a derivative of model system 2). This model system can be exploited using MC/BD to measure the closing rates of the fast gating in ClC as they depend on the intracellular and extracellular chloride concentration. Chen et al. (2003) measured the closing and opening rate dependence on intracellular and extracellular chloride concentration and proposed a foot-in-the-door mechanism for closing the channel. Our calculations can be used to test this hypothesis. Also, if a mechanism for the opening of the fast gate is elucidated from our PMF calculations, this mechanism can be checked by measuring the opening rate using MC/BD.

In regards to the basic MC/BD model, an inhomogeneous dielectric environment needs to be incorporated. This can be done via the empirical formula devised by Cheng et al. that reduces the complexity of addressing dielectric inhomogeneity on the interaction of two charged particles to a two-body, Coulomb-like term using the dielectric self energy of the permeating ions (which can be computed quickly and efficiently, prior to the BD simulation) (Mamonov et al., 2003; Cheng et al.).

REFERENCES

A. Accardi and M. Pusch. "Conformational changes in the pore of ClC-0." *J. Gen. Physiol.* **122**:277-93 (2003).

A.S. Arseniev, I.L. Barksukov, A.L. Lomize, V.Y. Orekhov, and V.F. Bystrov. "Refinement of the special structure of the gramicidin A transmembrane ion-channel." *Biol. Membr.* (USSR) **18**: 182 (1992).

J. Yin, Z. Kuang, U. Mahankali, and T.L. Beck. "Ion Transit Pathways and Gating in ClC Chloride Channels." *Proteins: Structure, Function, and Bioinformatics.* (in press).

A.E. Cardenas, R.D. Coalson, and M.G. Kurnikova. "Three-dimensional Poisson-Nernst-Planck theory studies: Influence of membrane electrostatics on gramicidin A channel conductance." *Biophys. J.* **79**, 80-93 (2000).

D. Chandler. *Introduction to Modern Statistical Mechanics.* Oxford University Press. (1987).

S. Chandrasekar, S. "Stocastic problems in physics and astrophysics." *Rev. Mod. Phys.* **15**: 1-89.

M.F. Chen, and T.Y. Chen. "Different fast-gate regulation by external Cl- and H+ of the muscle-type ClC chloride channels." *J. Gen. Physiol.* **118**, 23-32 (2001).

T.Y. Chen. "Coupling gating with ion permeation in ClC channels." *Science STKE* (www.sstke.org/cgi/content/full/sigtrans;2003/188/pe23, 2003).

T.Y. Chen, M.F. Chen, & C.W. Lin. "Electrostatic control and chloride regulation of the fast grating of ClC-0 chloride channels." *J. Gen. Physiol.* **122**, 641-651 (2003).

M. Cheng and R.D. Coalson. "Effective Ion-Ion Pair Potentials in Dielectrically Inhomogeneous Media: Applications to Ion Permeation through Model Pores." (in preparation).

S.H. Chung and S. Kuyucak. "Predicting channel function from channel structure using Brownian dynamics simulations." *Clinical and Experimental Pharmacology and Physiology.* ***28***: 89-94 (2001).

J. Cohen and K. Schulten. "Mechanism of Anionic Conductance across ClC." *Biophys. J.* **86**: 836-45 (2004).

P.S. Crozier, D. Henderson, R.L. Rowley, and D.D. Busath. "Model channel ion currents in NaCl-extended simple point charge water solution with applied-field molecular dynamics." *Biophys. J.* **81:**3077-3089 (2001).

D.A. Doyle, J.M. Cabral, R.A. Pfuetzner, A. Kuo, J.M. Gulbis, S.L. Cohen, B.T. Chait, and R. MacKinnon. "The Structure of the Potassium Channel: Molecular Basis of K^+ Conduction and Selectivity." *Science*. **280**: 69-77 (1998).

R. Dutzler, E.B. Campbell, M. Cadene, B.T. Chai, and R. MacKinnon. "X-ray structure of ClC chloride channel at 3.0 A reveals the molecular basis of anion selectivity." *Nature*. **415**: 287-94 (2002).

R. Dutzler, E.B. Campbell, and R. MacKinnon. "Gating the Selectivity Filter in ClC Chloride Channels." *Science.* **300**: 108-12 (2003).

W. Im, S. Seefedl, and B. Roux. "A Grand Canonical Monte Carlo-Brownian dynamics algorithm for simulation ion channels." *Biophys. J.* **79**: 788-801.

T.J. Jentsch. "Cell biology: Chloride channels are different." *Nature.* **415**:276-7 (2002).

L. Kalé, R. Skeel, M. Bhandarkar, R. Brunner, A. Gursoy, N. Krawetz, J. Phillips, A. Shinozaki, K. Varadarajan, and K. Schulten. "NAMD2: greater scalability for parallel molecular dynamics." *J. Comp. Phys.* **151**:283-312.

J.G. Kirkwood. "Statistical mechanics of fluid mixtures." *J. Chem. Phsys.* **3**:300-13.

S. Kumar, D. Bouzida, R.H. Swendsen, P.A. Kollman, and J.M. Rosenberg. "The Weighted Histogram Analysis Method for Free-Energy Calculations on Biomolecules. I: The Method." *J. Comp. Chem.* **13**:1011-21 (1992).

M.G. Kurnikova, R.D. Coalson, P. Graf, and A. Nitzan. "A lattice relaxation algorithm for three-dimensional Poisson- Nerst-Planck theory with application to ion transport through the gramicidin A channel." *Biophys. J.* **76**, 642-656 (1999).

A.R. Leach. *Molecular Modeling: Principles and Applications.* Prentice Hall. (2001).

A. D. Mackerrel Jr., D. Bashford, M. Bellot, R.L. Dunbrack Jr., J. Evanseck, M.J. Field, S. Fischer, J. Gao, H. Guo, S. Ha, D. Joseph, L. Kuchnier, K. Kuczera, F.T.K. Lau, C. Mattos, S. Michnick, T. Ngo, D.T. Nguyen, B. Prodhom, I.W.E. Reiher, B. Roux, M. Schlenkrich, J. Smith, R. Stote, J. Straub, M. Watanabe, J. Wiorkiewicz-Kuczera, D. Yin, and M. Karplus. "All-hydrogen empirical potential for molecular modeling and dynamics studies of proteins using the CHARM22 force field." *J. Phys. Chem. B.* **102**:3586-3616 (1998).

A. Mamonov, R.D. Coalson, A. Nitzan, and M. Kurnikova. "The role of the dielectric barrier in narrow biological channels: A novel composite approach to modeling single-channel currents." *Biophys. J.* **84**, 3646-61 (2003).

D. A. McQuarrie. *Statistical Mechanics.* Harper Collinx Publishers. (1976).

C. Miller. "Open-state substructure of single chloride channels from *Torpedo* electroplax." *Phil. Trans. R. Soc. Lond. B.* **299**: 401-11 (1982).

C. Miller and M.M. White. "A voltage-gated Cl^- conductance channel from *Torpedo* electroplax membrane." *Ann. N.Y. Acac. Sci.* **341**: 534-51 (1980).

C. Miller and M.M. White. "Dimeric structure of single chloride channels from *Torpedo* electroplax." *Proc. Natl. Acad. Sci. USA.* **81**: 2772-5 (1984).

G.V. Miloshevsky, and P.C. Jordan. "Anion Pathway and Potential Energy Profiles along Curvilinear Bacterial ClC Cl^- Pores: Electrostatic Effects of Charged Residues." *Bophys. J. 86*: 825-35 (2004).

M. Pusch, U. Ludewig, and T.J. Jentsch. "Temperature dependence of fast and slow gating relaxations of ClC-0 chloride channels." *J. Gen. Physiol.* **109**: 105-16 (1997).

M. Pusch, U. Ludewig, A. Rehfeldt, and T.J. Jentsch. "Gating of the voltage-dependent chloride channel ClC-0 by the peremeant anion." *Nature.* **373**: 527-31 (1995).

B. Roux. "The calculation of the potential of mean force using computer simulations." *Comp. Phys. Comm.* **91**:275-82 (1995).

B. Roux. "Theoretical and computational models of ion channels." *Curr. Opin. Struct. Biol.* **12**, 182-189 (2002).

L. Song and E. Gouaux. "Crystallization of the alpha-hemolysin heptamer solubilized in decyldimethyl and decyldiethylphosphine oxide." *Acta. Crystallogr. D. Biol Crystallogr.* **54**: 276-278 (1998).

J.P. Valleau and D.N. Card. "Monte Carlo Estimation of the Free Energy by Multistage Sampling." *J. Chem. Phys.* **57**:5457-62 (1972).

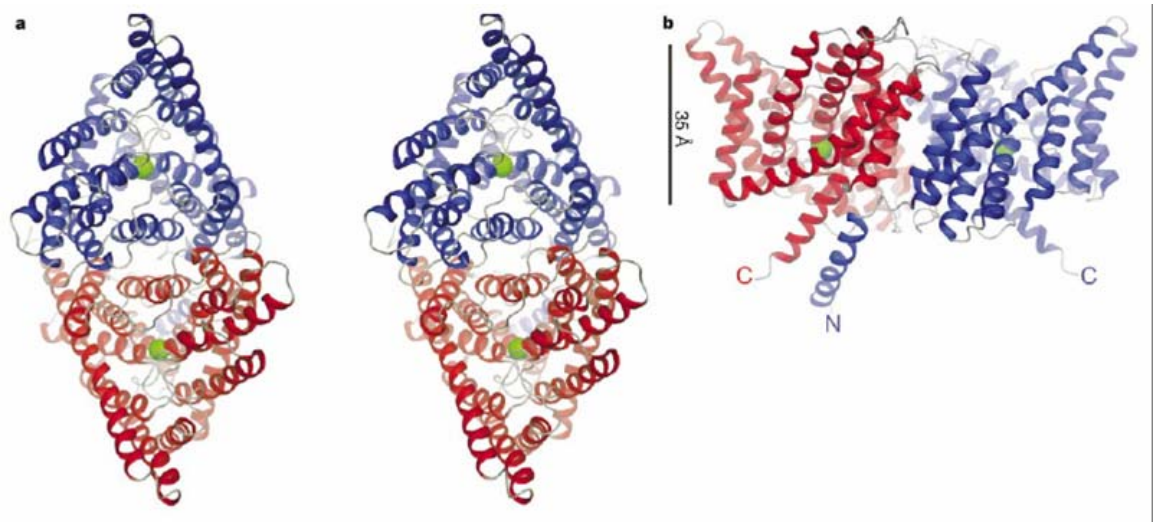

Figure 1: StClC Structure

Structure of StClC from Dutzler et al. (2002). "Structure of the StClC dimmer. **a**, Stereo view of a ribbon representation of the StClC dimer from the extracellular side. The two subunits are blue and red. A Cl^- ion in the selectivity filter is represented as a green sphere. **b**, View from within the membrane with the extracellular solution above. The channels is rotated by 90° about the x- and y- axis relative to **a**. The black line (35 Å) indicates the approximate thickness of the membrane."

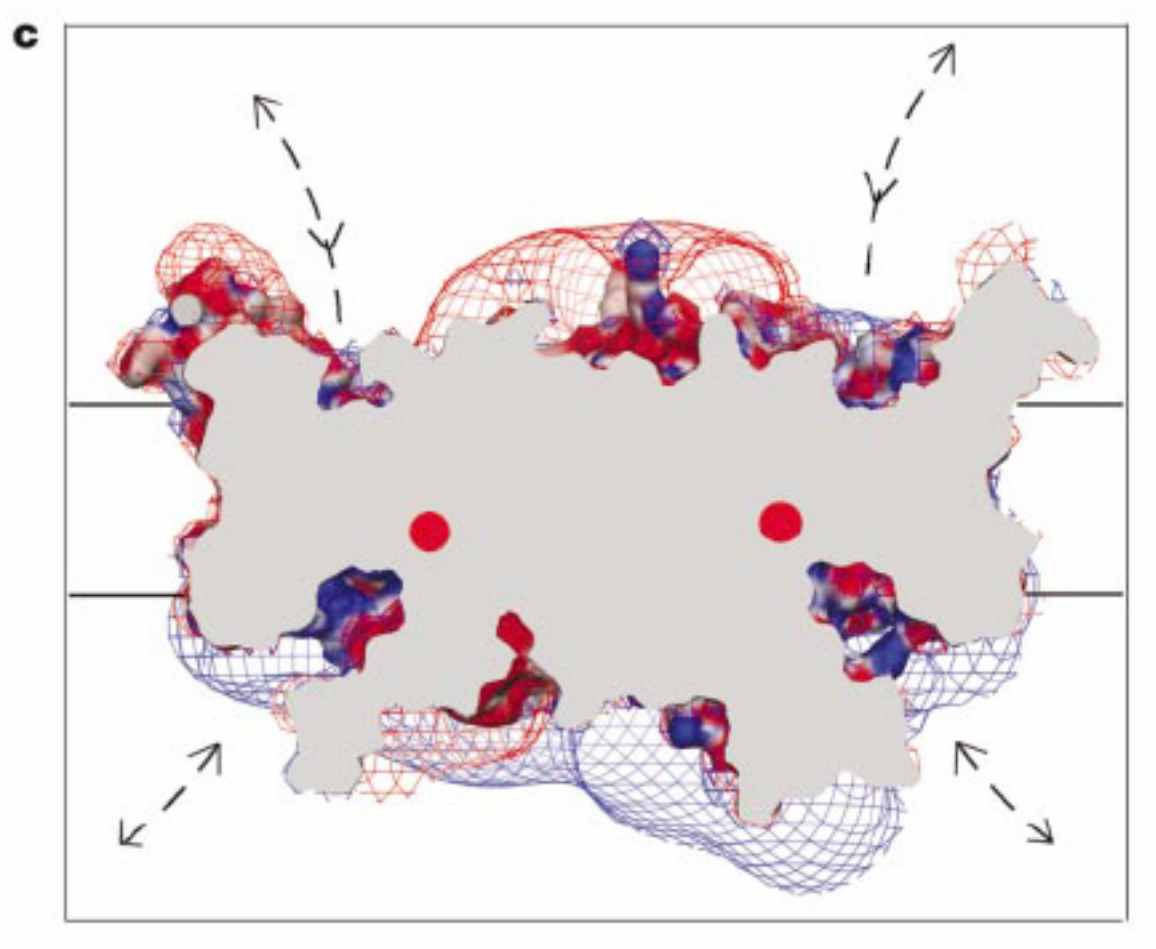

Figure 2: Permeation Path in StClC

Peremeation path through ClC suggested by Dutzler et al. (2002). "Surface electrostatic potential on the ClC dimer in 150 mM electrolyte. The channel is sliced in half to show the pore entryways (but not the full extent of their depth) on the extracellular (above) and intracellular (below) sides of the membrane. Isocontour surfaces of -12 mV (red mesh) and +12 mV (blue mesh) are shown. Cl^- ions are shown as red spheres. Dashed lines highlight the pore entryways."

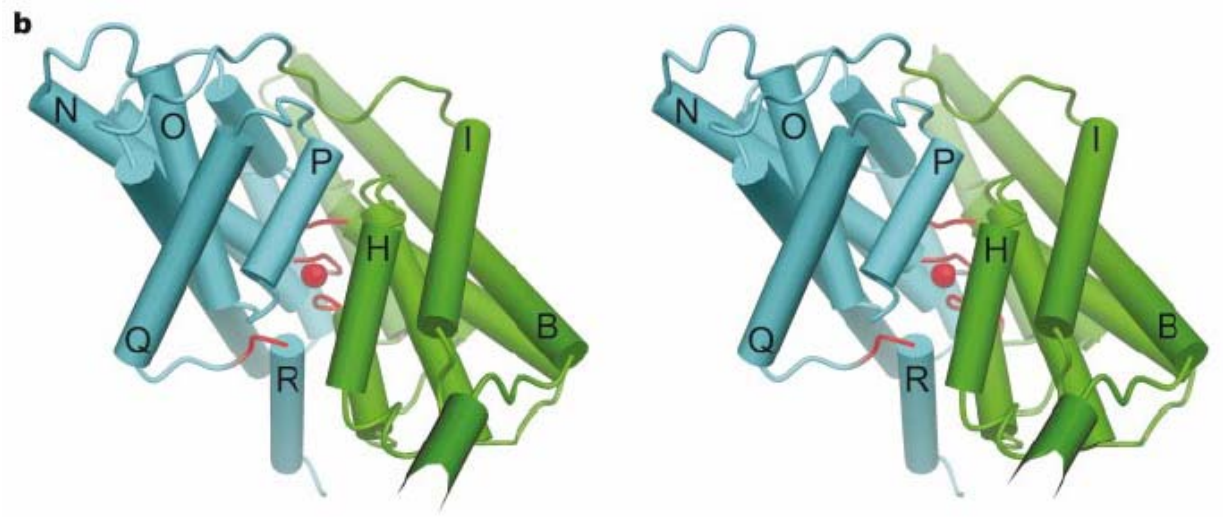

Figure 3: StClC Monomer Structure

StClC Monomers from Dutzler et al. (2002). "Stereo view of the StClC subunit viewed from within the plane of the membrane from the dimer interface with the extracellular solution above. The α-helices are drawn as cylinders, loop regions as cords (with the selectivity filter red), and the Cl^- ion as a red sphere."

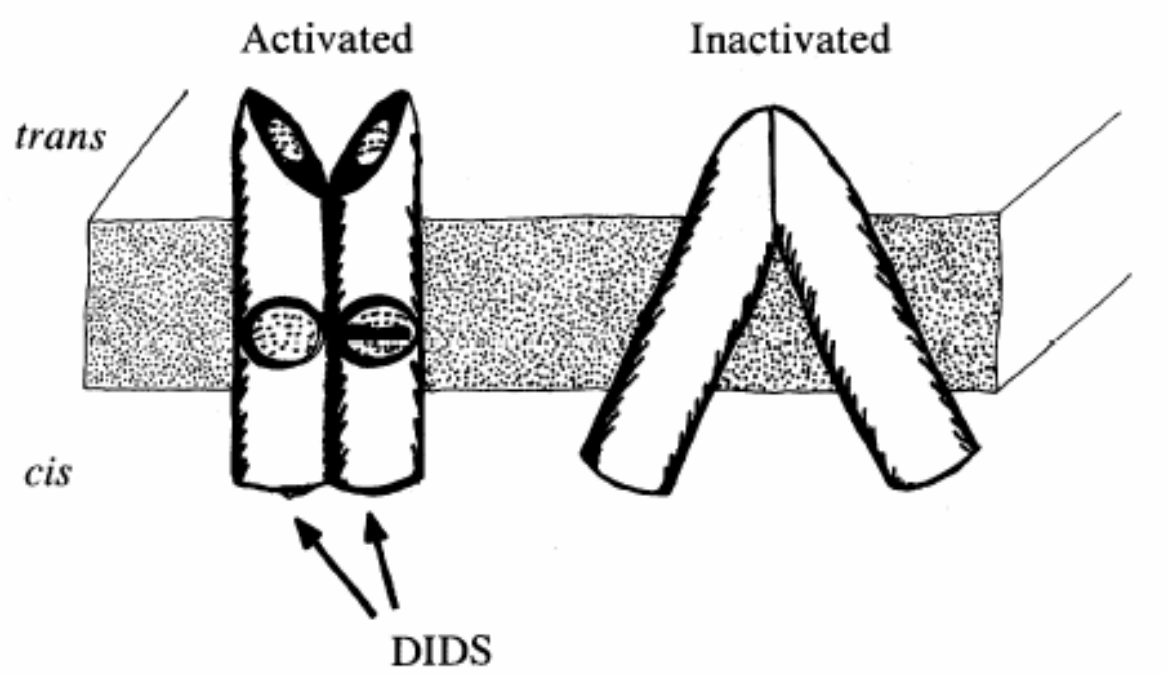

Figure 4: Cartoon of Slow Gating in ClC

Cartoon of ClC-0 slow gating mechanism taken from Miller et al. (1984).

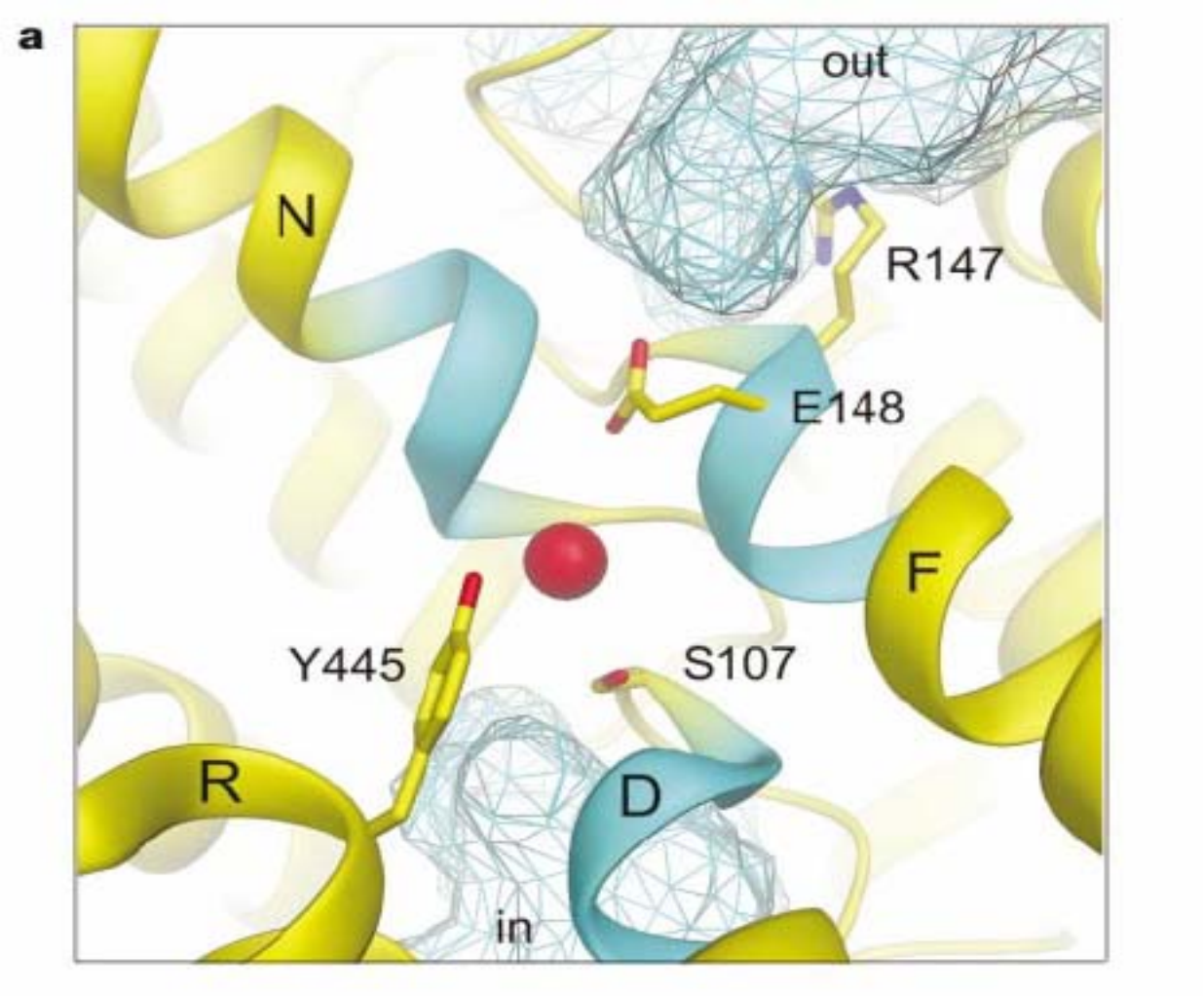

Figure 5: StClC Gating Region and Selectivity Filter

Chloride binding site of StClC and the fast gate (E148) from Dutzler et al. (2002). "The ion-binding site viewed from the dimer interface, along the pseudo two-fold axis, with foreground α-helices removed for clarity. The protein is shown as a ribbon with selected residues as sticks. The amino terminal ends of α-helices D, F and N are cyan and Cl^- is shown as a red sphere. Aqueous cavities approaching the selectivity filter from the extracellular solution (out) and intracellular solution (in) are shown as a cyan mesh."

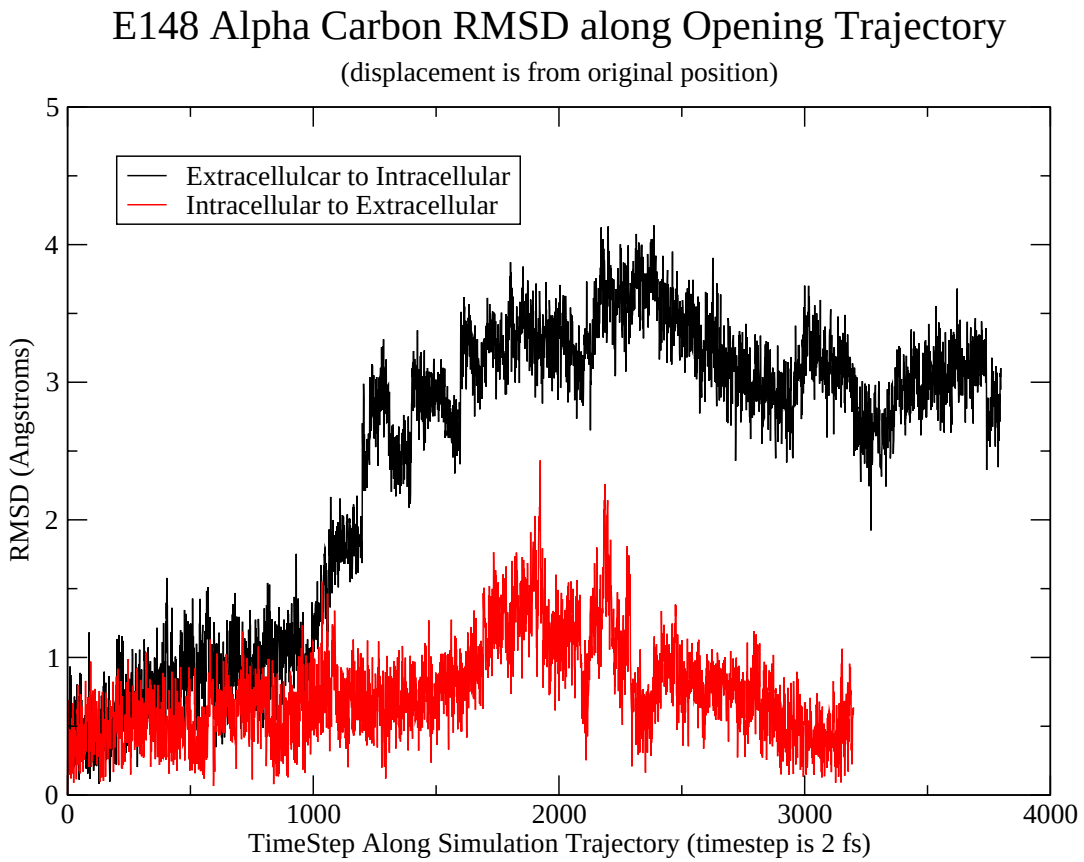

Figure 6: Backbone RMSD at Glutamate Gate

Root mean squared distance (RMSD) of the alpha carbon of the glutamate gate (E148) of StClC versus the time-step of opening the StClC channel by moving a chloride ion from the extracellular to the intracellular side (black) and by moving a chloride ion from the intracellular to the extracellular side (red).

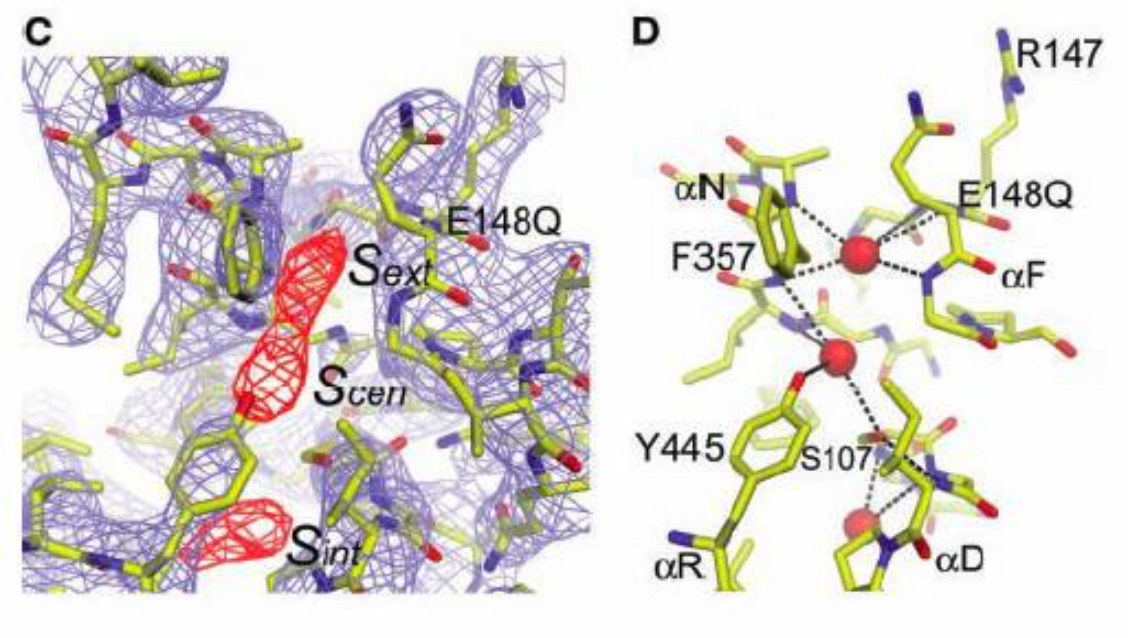

Figure 7: Selectivity Filter and Open Gate of EcClC E148Q Mutant

Structure of the E148Q mutant (glutamate mutated to glutamine) of EcClC from Dutzler et al. (2003). "(**C**) Electron density in the selectivity filter of the EcClC E148Q mutant at 3.3 Å. The map was calculated from native amplitudes and solvent-flattened two-fold averaged phases and is contoured at 1σ. An (F_{Br} - F_{Cl}) difference Fourier map at 4.1 Å, contoured at 4.5σ, is shown in red. (**D**) View of the ion-binding sites of the EcClC E148Q mutant. "

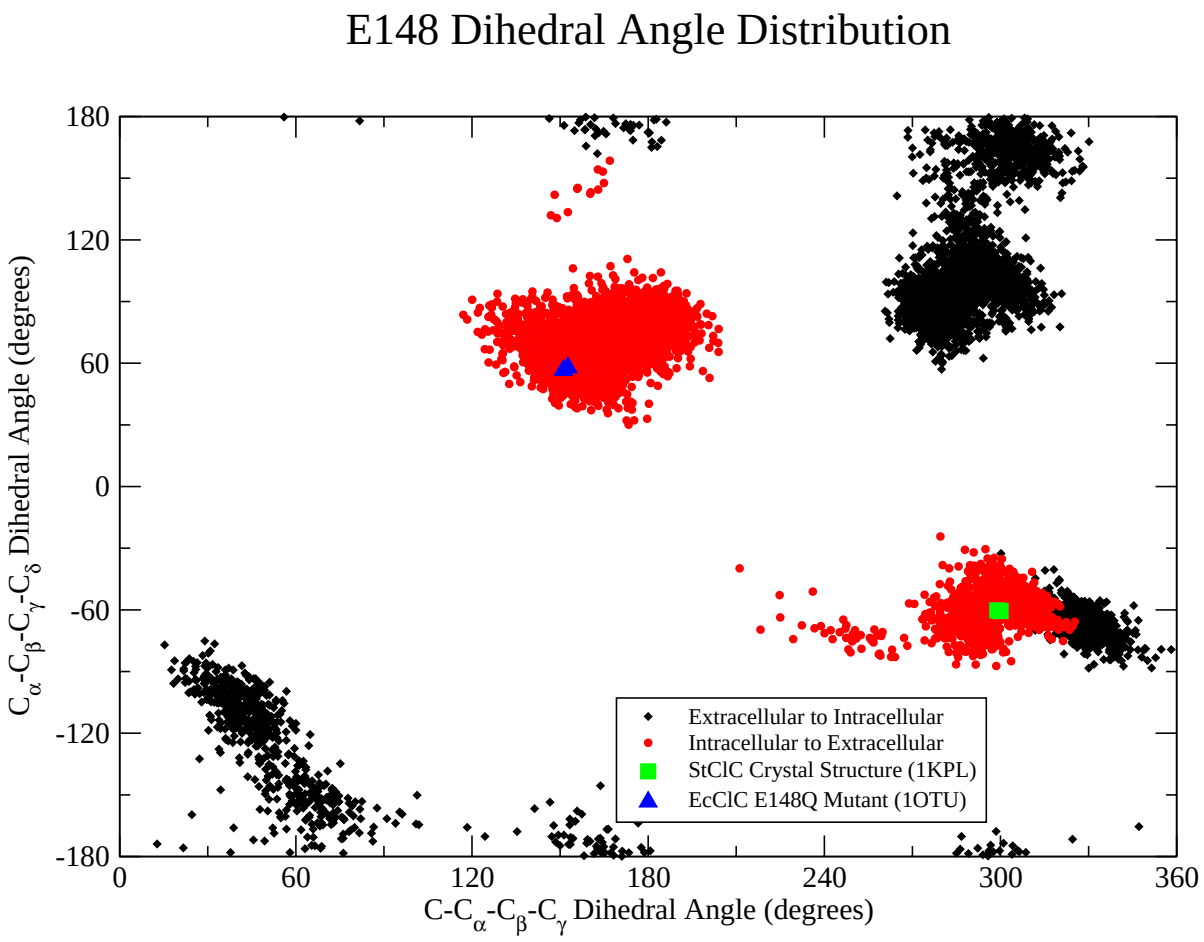

Figure 8: Distribution of Glutamate Side Chain Dihedrals

Dihedral angle distribution of the glutamate StClC gate (E148) from both the extracellular to intracellular (small black diamonds) and intracellular to extracellular (small red circles) trajectories. Each dot represents a snapshot taken every ps from the MD trajectory. Also, the dihedral angles of the same residue of the "closed" StClC crystal structure (two overlapping big green squares) and the "open" mutant (E148Q) EcClC structure (two overlapping big blue triangles) are plotted.

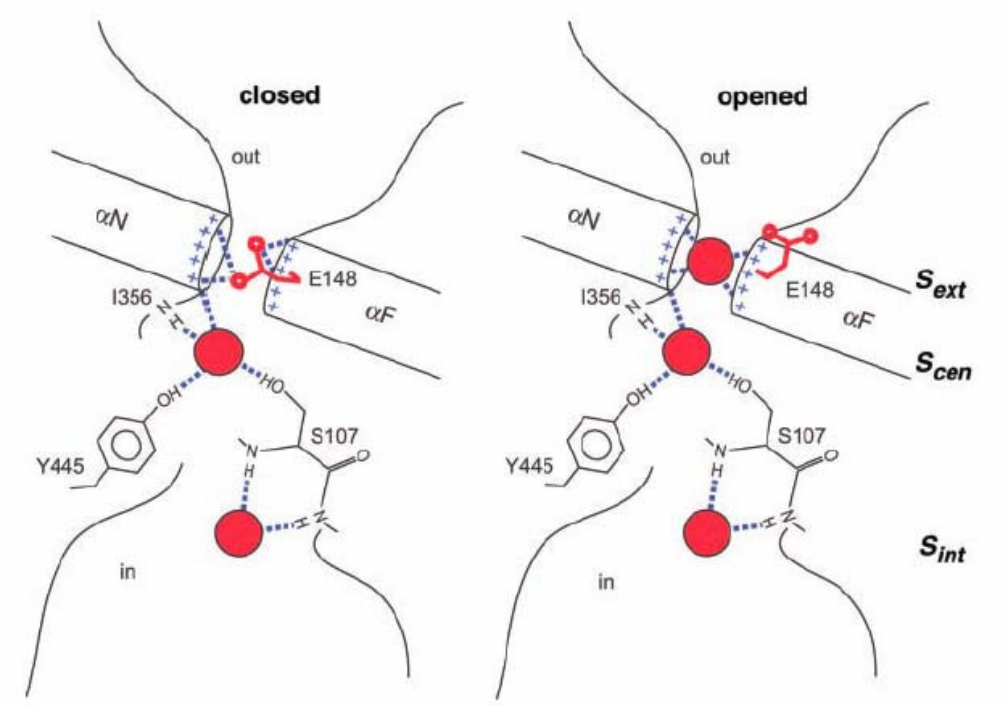

Figure 9: Cartoon of Fast Gating

"Schematic drawing of the closed and opened conformation of a ClC chloride channel. In the closed conformation, the ion-binding sites S_{int} and S_{cen} are occupied by chloride ions, and the ion-binding site S_{ext} is occupied by the side chain of Glu^{148}. In the opened conformation, the side chain of Glu^{148} has moved out of binding site S_{ext} into the extracellular vestibule. S_{ext} is occupied by a third chloride ion. Chloride ions are shown as red spheres, the Glu^{148} side chain is colored red, and hydrogen bonds are drawn as dashed lines." (Dutzler et al. 2003)

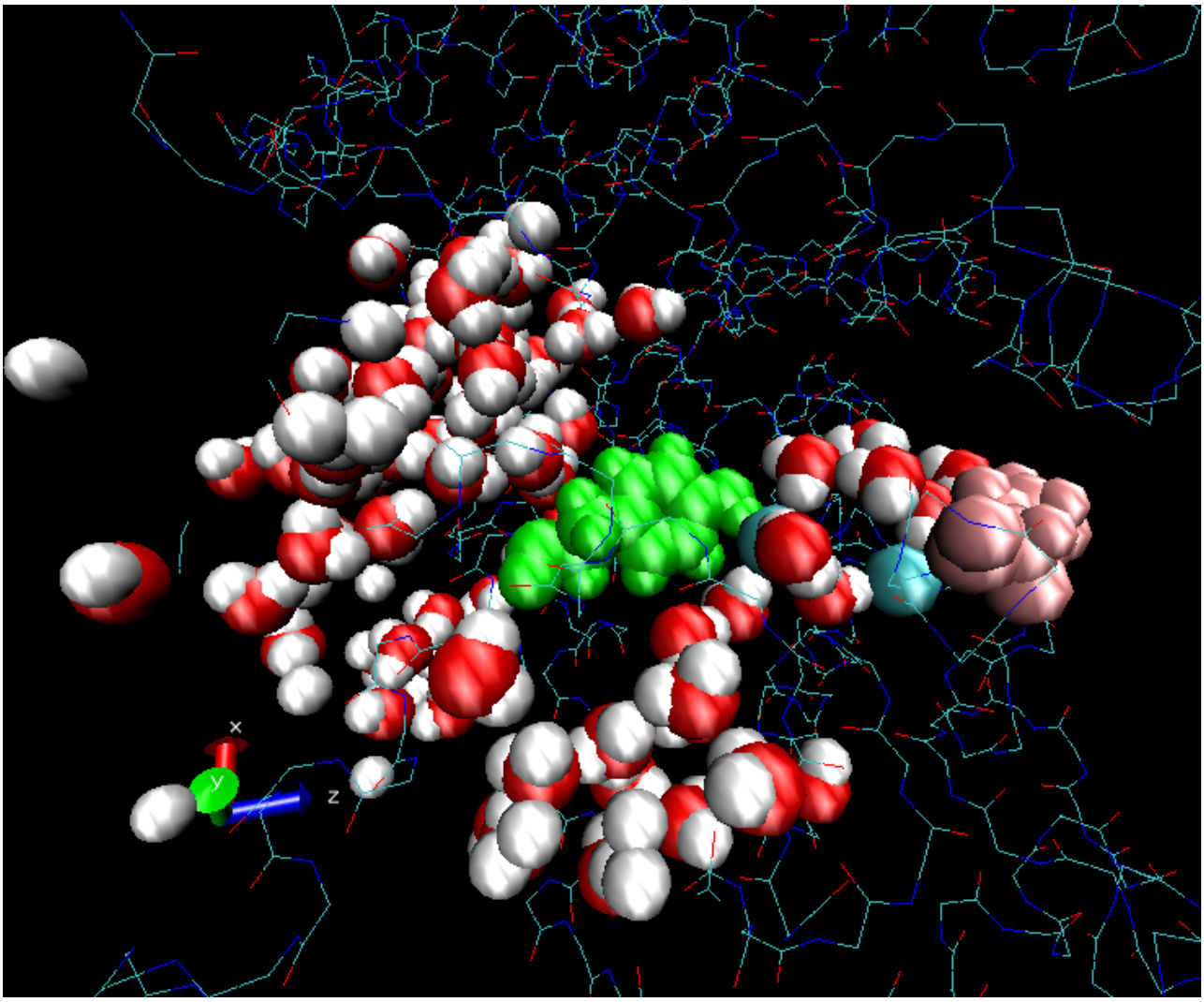

Figure 10: Permeation Path 1 for Extracellular to Intracellular Trajectory

Pore corresponding to that suggested by Dutlzer et al. (2002) and Cohen et al. (2004). The glutamate gate (E148) is shown in pink and a key tyrosine residue (Y445) on the intracellular side of the channel is shown in green. Selected water molecules in the pore are shown in red (oxygen) and white (hydrogen). A chloride ion near the glutamate gate is shown in blue-green color. The colored lines represent the backbone of the StClC channel.

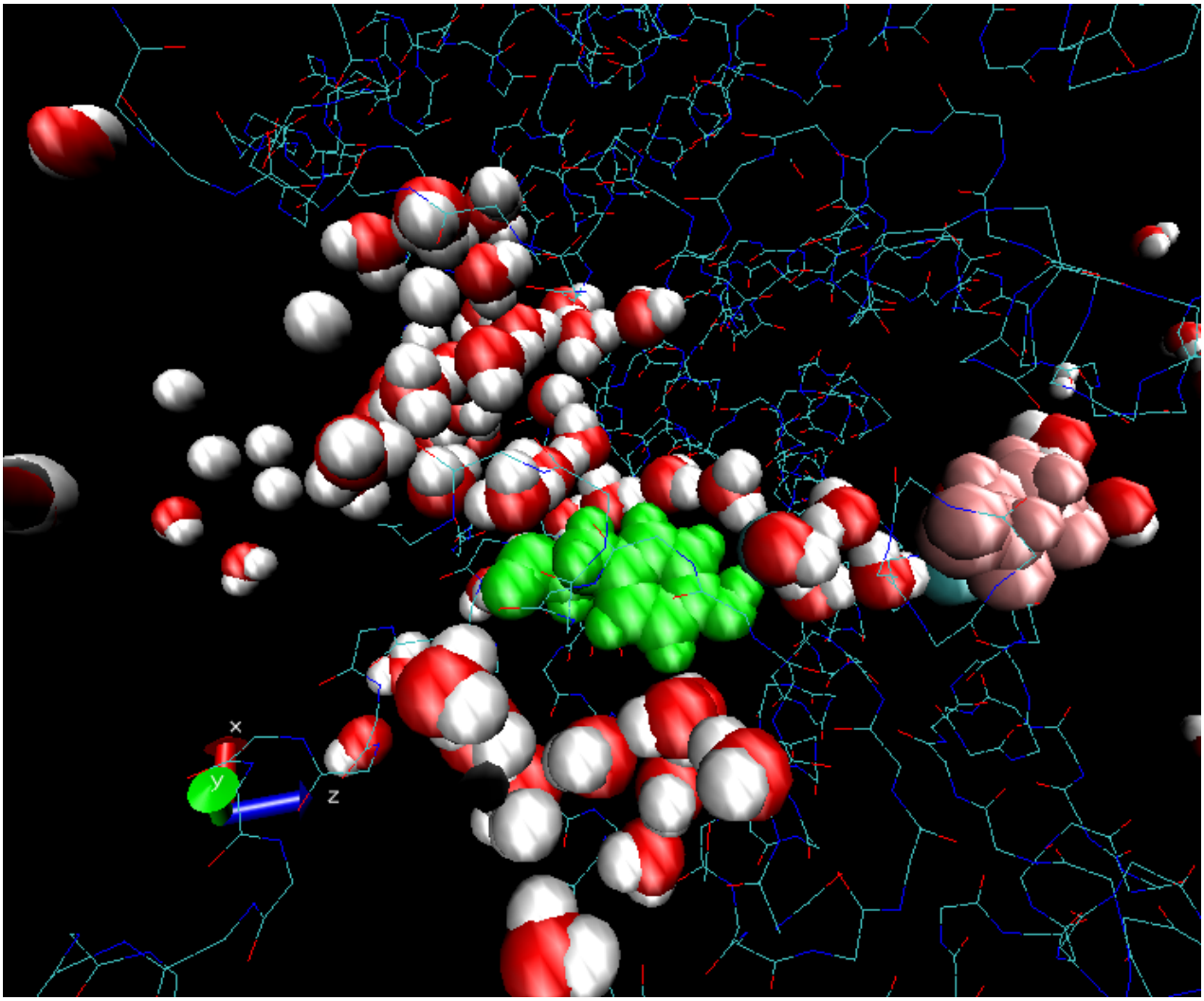

Figure 11: Permeation Path 2 for Extracellular to Intracellular Trajectory

Alternate pore for waters that branches off of the pore depicted in Figure 10. The glutamate gate (E148) is shown in pink and a key tyrosine residue (Y445) on the intracellular side of the channel is shown in green. Selected water molecules in the pore are shown in red (oxygen) and white (hydrogen). A chloride ion near the glutamate gate is shown in blue-green color. The colored lines represent the backbone of the StClC channel.

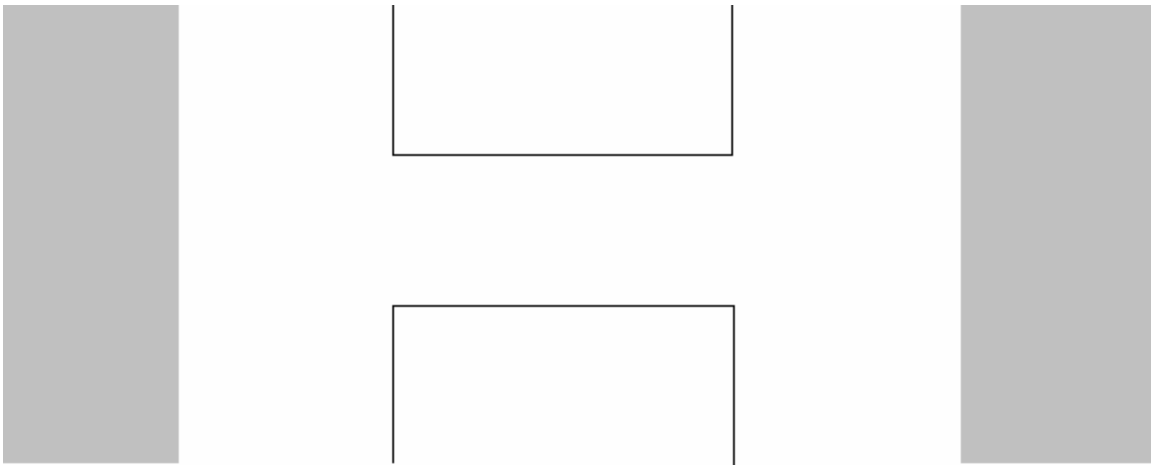

Figure 12: Diagram of Brownian Dynamic System

Diagram of model system for Brownian dynamics. The solid black line depicts the interface between the membrane and water. The shaded regions represent the portions of the reservoirs on each side of the membrane where a constant concentration of mobile ions is maintained.

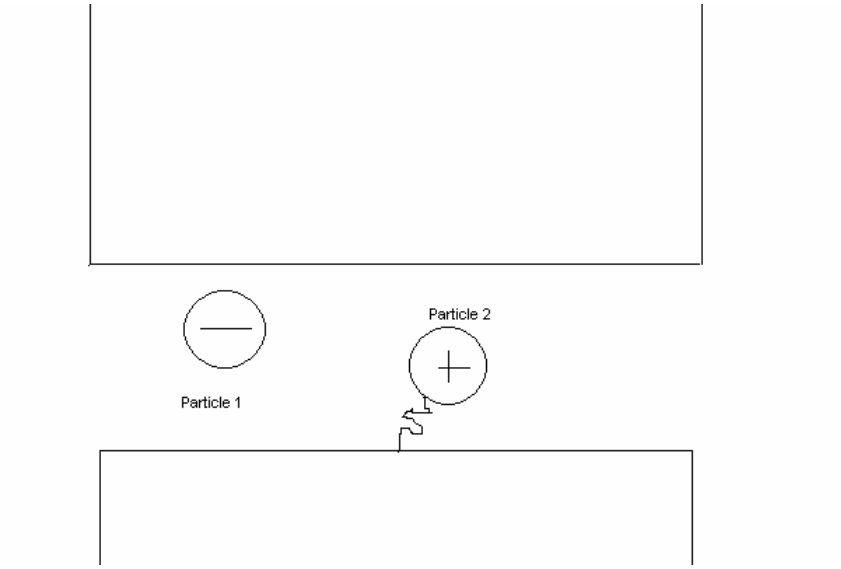

Figure 13: Diagram of Model System I

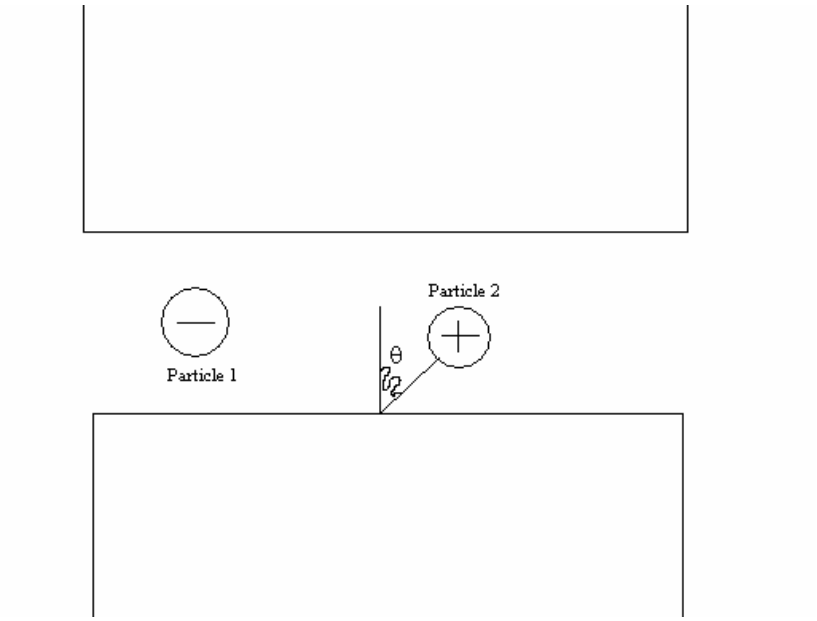

Figure 14: Diagram of Model System 2

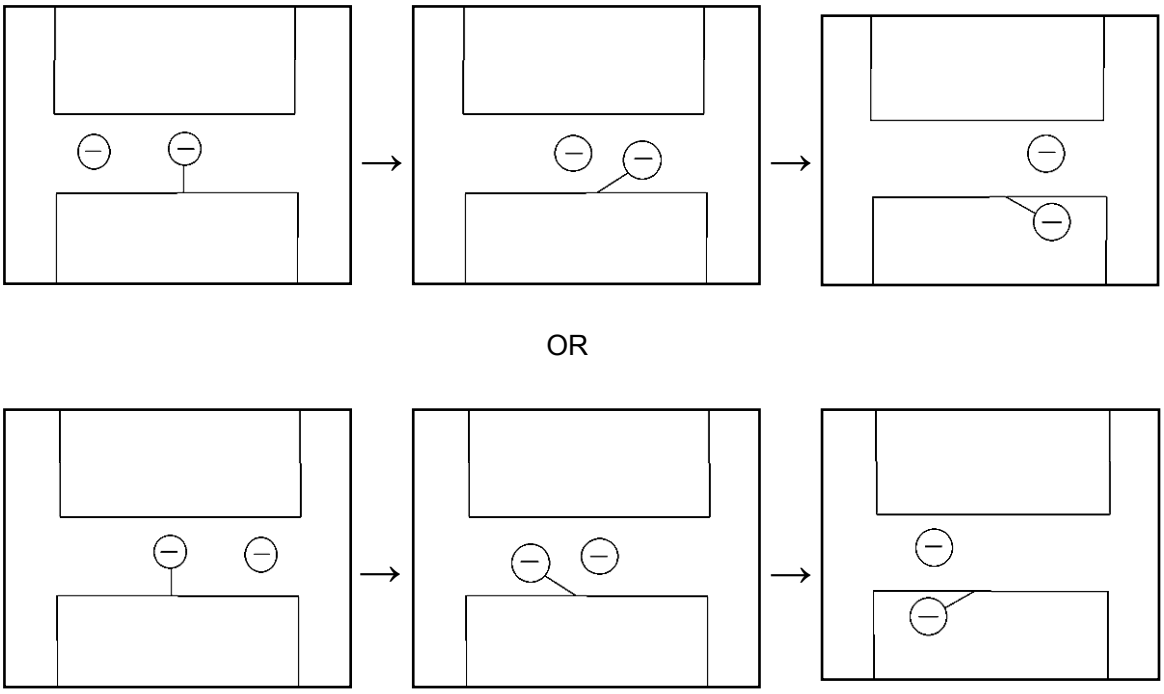

Figure 15: Diagram of Ion Permeation in Model System 2

Diagram of a particle interaction with the gate in model system 2. The top diagrams represent a permeant ion that originated from the left reservoir interacting with the gate. The bottom diagrams represent a permeant ion that originated from the right reservoir interacting with the gate. Note that final diagram on the top, and the initial diagram of the bottom show a solute particle in the same position; however, the gates of each diagram are in different positions and have a different set of accessible configurations.

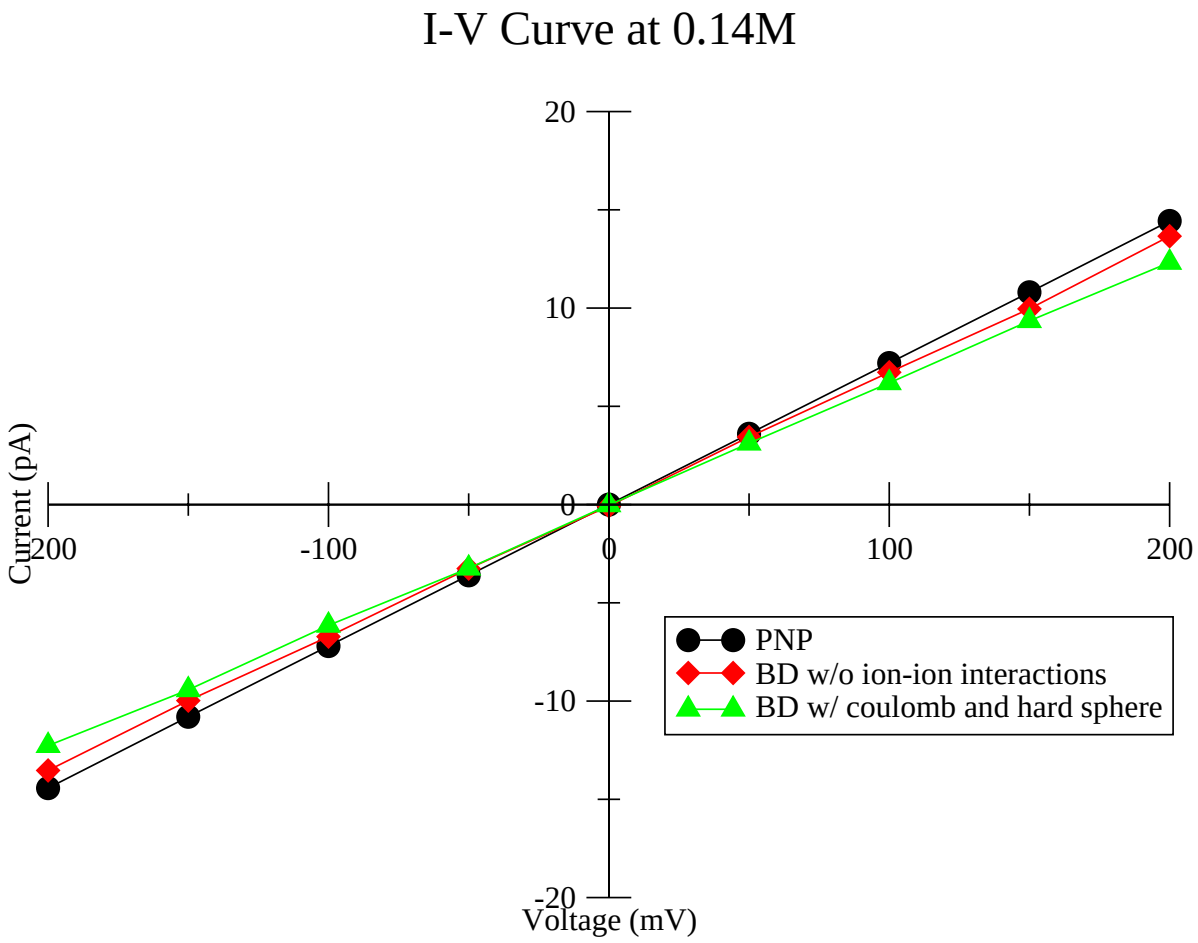

Comparison current-voltage curves calculated by PNP (black circles), BD without ion-ion interactions (red diamonds), and BD with ion-ion interactions (green triangles) for a simple pore system (no gate).

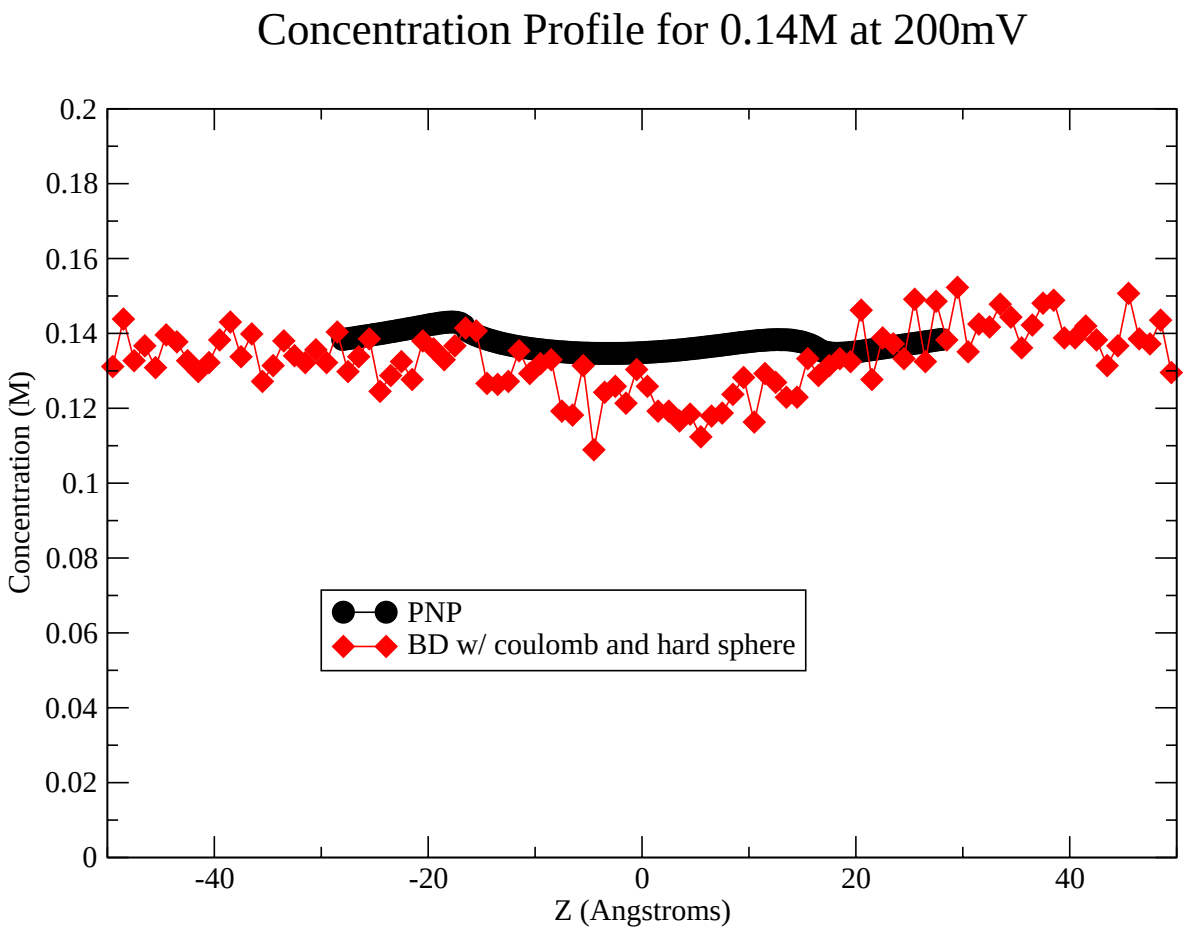

Figure 17: Comparing Concentration Profiles of Bare PNP and BD

Comparison between the concentration profiles computed with PNP and BD with ion-ion interactions for a simple pore system (no gate) with a 200 mV applied potential.

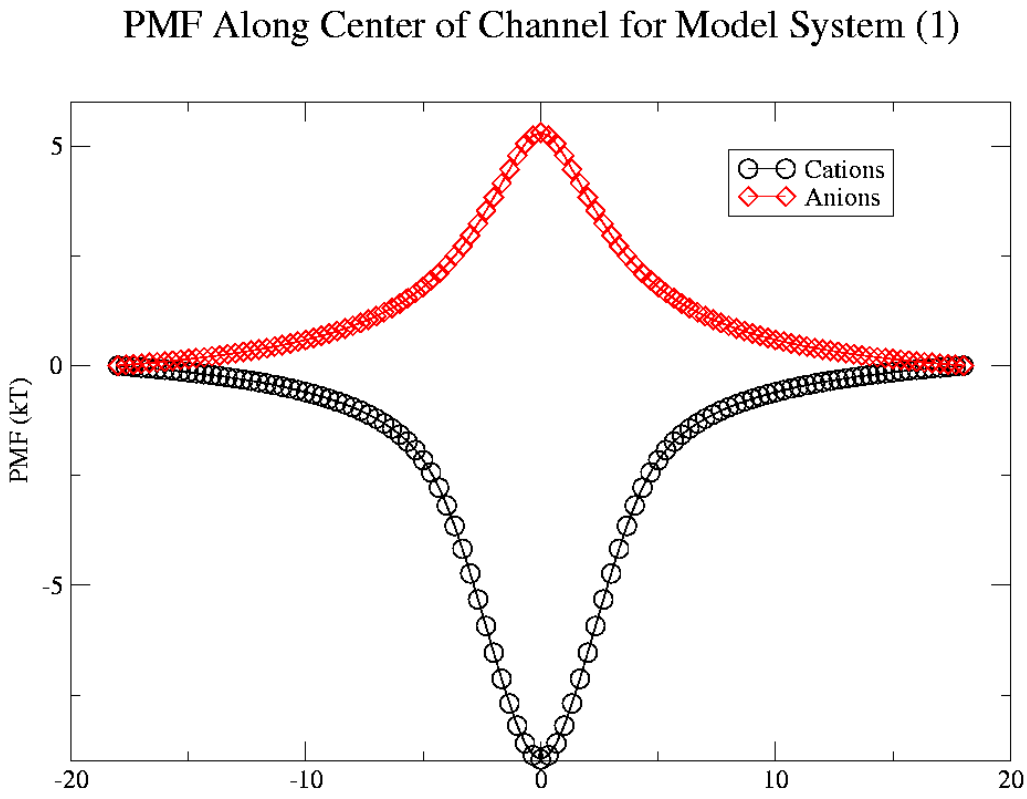

Figure 18: PMF for Model System I

The potential of mean force (PMF) of anions and cations along the channel axis as computed for model system 1.

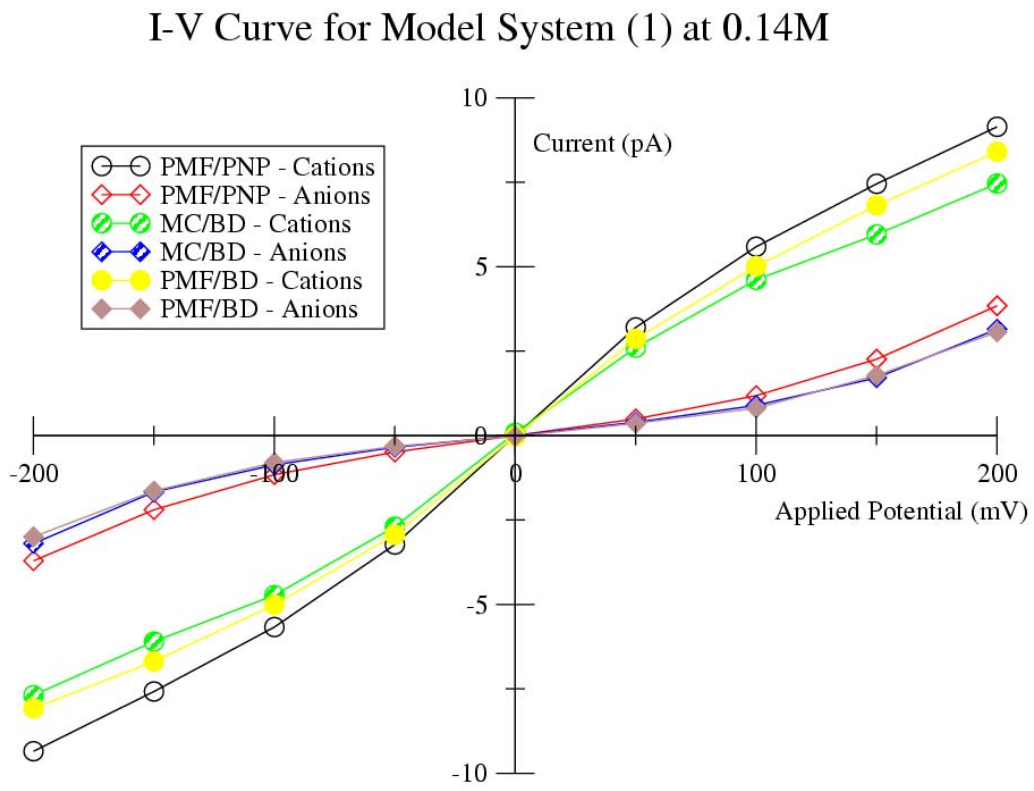

Figure 19: I-V Curves for Model System I

Comparison of current-voltage curves computed by PMF/PNP, MC/BD, and PMF/BD for model system 1.

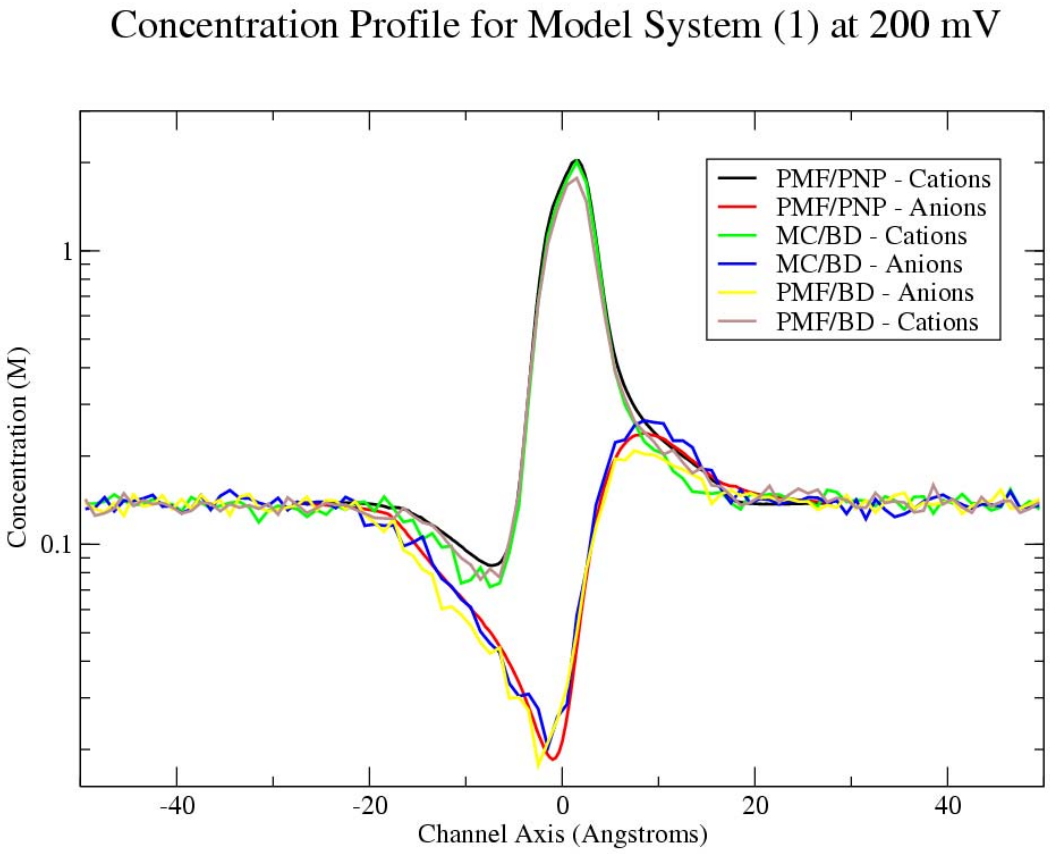

Figure 20: Concentration Profiles for Model System I

Comparison of concentration profiles for permeating ions in model system 1 computed by PMF/PNP, MC/BD, and PMF/BD with an applied potential of 200mV.

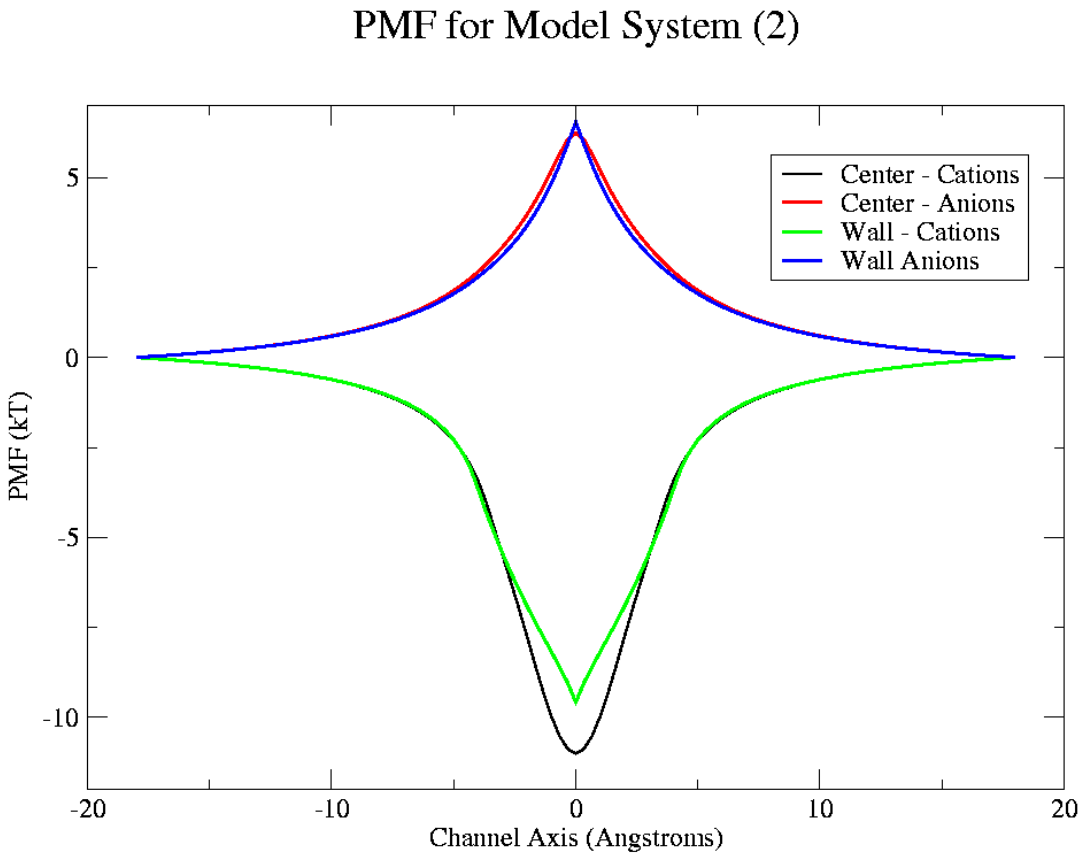

Figure 21: PMF for Model System 2

The potential of mean force (PMF) of anions and cations in model system 2 along the channel axis and along the wall of the channel.

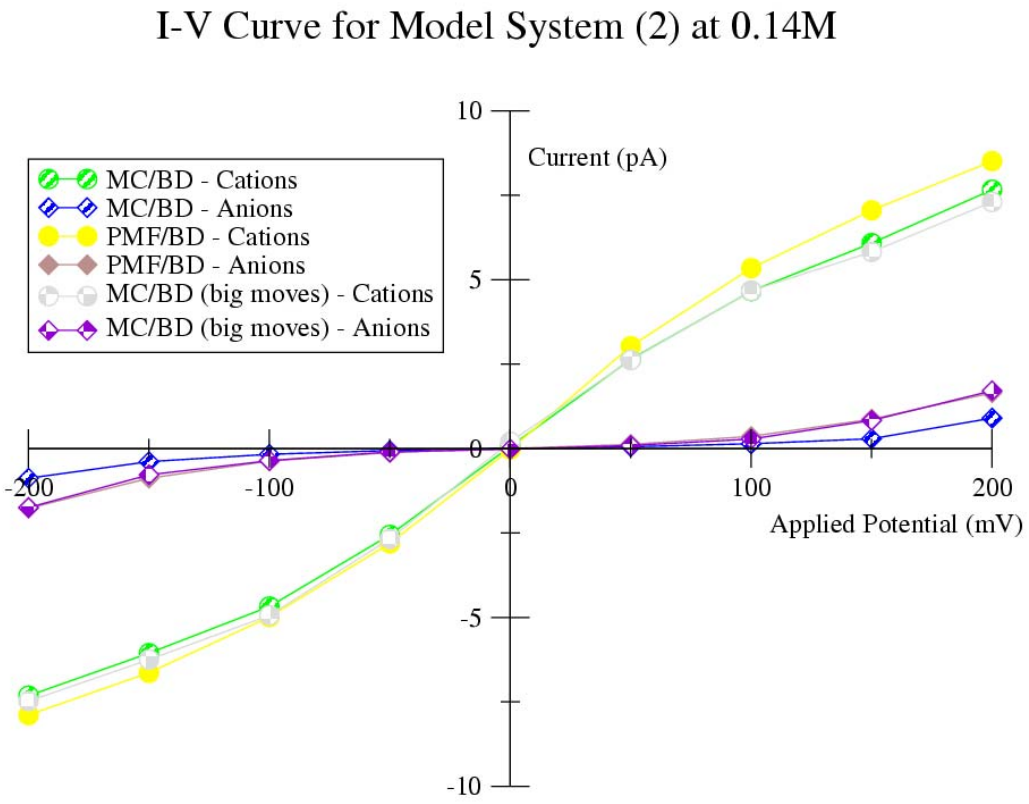

Figure 22: I-V Curves for Model System 2

Comparison of current-voltage curves computed by PMF/PNP, MC/BD (using small MC moves and big MC moves), and PMF/BD for model system 2.

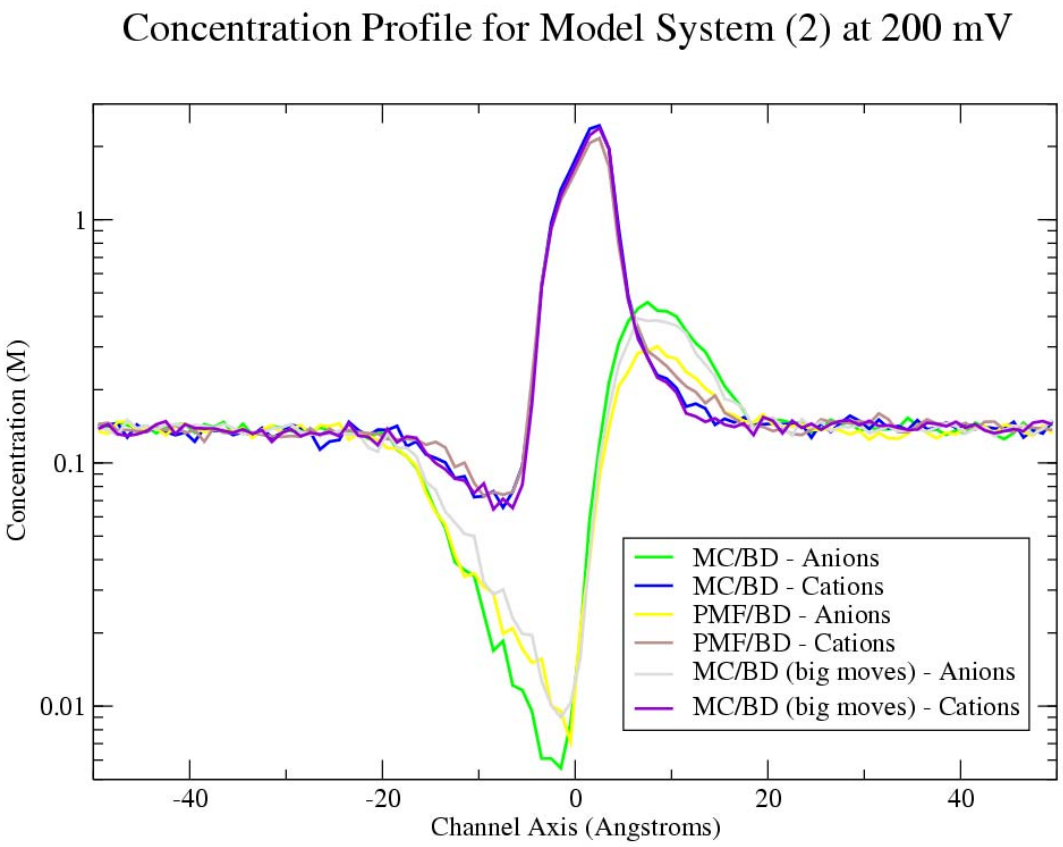

Figure 23: Concentration Profiles for Model System 2

Comparison of concentration profiles for permeating ions in model system 2 computed by PMF/PNP, MC/BD (using small MC moves and big MC moves), and PMF/BD with an applied potential of 200mV.